Delamination or slab detachment beneath Vrancea? New arguments from local earthquake tomography

by

Ivan Koulakov (1, 2),
Bogdan Zaharia (3),
Bogdan Enescu (4),
M. Radulian (3),
M. Popa (3),
Stefano Parolai (2)
and J. Zschau (2)

1. Institute of Petroleum Geology and Geophysics, Novosibirsk, Russia
(KoulakovIY@ipgg.nsc.ru)
2. GFZ German Research Centre for Geosciences, Potsdam, Germany
3. National Institute for Earth Physics (NIEP), Bucharest, Romania
4. National Research Institute for Earth Science and Disaster Prevention (NIED), Tsukuba, Japan

G-cube
Manuscript number 2009GC002811

Potsdam, Bucharest, Novosibirsk, Tsukuba
November, 2009

Abstract

Vrancea, located at the South-Eastern Carpathians Arc bend, is one of the areas in the Alpine-Himalayan belt that features strong earthquakes occurring at intermediate depths (60 – 200 km). In this study we investigated the crustal and lithospheric structure beneath the Vrancea seismic area using a local earthquake tomography approach. We used an updated and revised catalog, spanning from 1982 to 2006, that uses data from both permanent and temporary networks in the target area. Simultaneous tomographic inversion for the Vp and Vs anomalies and the Vp/Vs ratio and source locations was done using the LOTOS code. The reliability and robustness of the results were rigorously checked using various tests (e.g., by studying the role of different parameters on the results of the inversion, performing the inversion using random data subsets, synthetic modeling). The tomography results clearly indicate the presence of a high velocity material beneath Vrancea at a depth interval of about 60 to 200 km that coincides with the distribution of intermediate depth seismicity. This result agrees generally with previous tomographic studies. We compare two scenarios leading to this structure: (1) subduction and slab detachment and (2) "drop-forming" or delamination. The latter mechanism presumes that the thickening of the crust due to continent-continent collision causes transformation of the mafic lower crust into denser eclogite. This material accumulates until it reaches a critical mass, at which point it forms a large drop that begins to fall down. We propose that the high velocity anomaly we observe in our tomogram might represent the descending eclogitic lower crust material enveloped by the entrained lithosphere. It is possible that a similar delamination process can be observed in other parts of the Alpine-Himalayan belt, such as in the Pamir Hindu-Kush area.

Key words: seismic tomography, Vrancea (Romania), delamination, slab detachment

1. Introduction

The interaction of lithospheric plates is one of the most important and intriguing geological processes on Earth. Collisions of ocean-ocean and ocean-continent plates occur through the subduction of the oceanic plates, and their general mechanism is roughly understood and accepted by most scientists. On the contrary, many aspects of continent-continent collisions remain enigmatic. In some continental areas, collisions of continental plates cause considerable surface shortening that may reach several hundred kilometers (e.g., in Central Asia due to the India-Asia collision). Many questions related to this topic are actively debated. For example, what happens to the mantle section of the continental lithosphere during the continent shortening? In such cases we usually observe a coupling of the crust, but the lithospheric mantle does not increase in thickness. Why is the stable cratonic-type lithosphere usually thicker than that in the collision belts? Why is the lithosphere in these belts not coupled? What is the mechanism for recycling the mantle continental lithosphere? Does it sink, like the oceanic lithosphere?

In some collisional areas of continental Asia, intermediate depth seismicity at depths of more than 100 km is observed (e.g. Pamir-Hindu-Kush, Zagros, Burma, and Vrancea). To explain this phenomenon, many authors draw a parallel with classical subduction of oceanic plates, presuming the existence of a sinking oceanic lithosphere in the upper mantle. For the areas of Zagros and Burma located close to oceanic basins, such a mechanism seems plausible. However, for the Pamir Hindu-Kush and Vrancea regions such an explanation is debatable, since there is no clear evidence of oceanic basins existing in these regions in the recent past (e.g. less than 10 MA). In this paper we conduct a local tomography study for the Vrancea region and based on our results, we try to find out which mechanism is most probable for the Vrancea region. The conclusions made in this case may be generalized for explaining the mechanisms of lithosphere recycling also in other cases of continent-continent collision.

Understanding the nature of tectonic processes that take place in the highly populated areas of the Alpine mountain system is also important for mitigating seismic risk in the region. The most intriguing feature of the Vrancea region is the very active intermediate-depth seismicity, densely concentrated in a vertically oriented cluster below a depth of 60 km. Strong earthquakes ($M > 7.0$) that can produce significant damage over large areas occur periodically in this deep cluster (there are roughly 2 – 3 earthquakes per century). Although many different multidisciplinary geological and geophysical studies have been performed in the Vrancea region, the nature of the intermediate-depth seismicity cluster is still actively debated. In the next section we will present the important current concepts and ideas that are proposed to explain the occurrence of Vrancea earthquakes.

As will be shown in the next section, the deep structure beneath the Vrancea region has been previously studied by many authors. At the same time we claim that in the present work we have achieved a certain progress in respect to previous studies. First of all, in this study, we used a newly updated local earthquake dataset with higher amount and quality of picks than in previous studies. This allowed for a more refined image of the underground structure in the Vrancea region. Second, we used a code for tomographic inversion and source location, LOTOS (*Koulakov*, 2009), which has some particular features not present in the codes used in previous studies (see section 3). We verified the results by performing many different robustness and synthetic tests (see Appendices A1-A5). They were also used to evaluate the optimal values of the free parameters used in the inversion and estimate the spatial resolution of the resulting model.

It is worth noting that seismic tomography still remains an imperfect tool, and different authors often provide non-coherent images for the same areas and even for the same datasets. Thus, performing independent inversions based on independent algorithms and data helps to identify the most robust results and provides important information for the validation of different seismotectonic models.

2. Geotectonic setting of the area and previous seismic studies

The Vrancea region is part of the Carpathian mountain system, which, in turn, represents a northeastern branch of the Alpine fold-and-thrust system (Figure 1). The tectonic development of the Alpine system began in the Jurassic and is mostly controlled by the collision of three large continental plates: the Eurasian, African, and Arabian. This collision caused the formation of extremely complex tectonic structures, consisting of many microplates and folded belts. The Carpathian orogenesis appears to be due to the shaping of the boundary of the East European Platform, which forms a loop in the Vrancea region (Figure 2). The Southeastern Carpathian Arc bend is located at the confluence of three main tectonic units (East-European plate, Intra-Alpine subplate and Moesian subplate) in the Vrancea region of Romania (Figure 1). The collision of this segment of the Alpine belt began in the Cenozoic as a result of the lateral eastward extrusion caused by the continuous convergence in Alps (*Ratschbacher et al.*, 1991). In the Vrancea region, an oceanic basin, floored by an oceanic crust, lays in the area of the present-day Carpathians which was consumed by subduction during Tertiary times (*Burchfiel*, 1976; *Csontos*, 1995; *Csontos and Voros*, 2004). A total width of 130 km of the basin was subducted during the first episode, with a convergence rate of approximately 2.5 cm yr^{-1} (*Roure et al.*, 1993; *Roca et al.*, 1995). The active shortening process stopped during the late Oligocene – Early Miocene periods

(about 20 MA) when all the oceanic-type basins were closed (*Ellouz and Roca*, 1994; *Linzer et al.*, 1998).

In contrast with the Eastern Carpathian branch, where the convergence of the plates seems to be currently inactive, complex active processes still take place beneath Vrancea in a very confined area. The brightest manifestation of this process is a cluster of intermediate seismicity beneath Vrancea in a narrow nearly vertical volume at depths below 60 km, which is clustered along a NE-SW direction (e.g., *Wenzel et al.,* 1996*, Radulian et al.*, 2008, *Radulian and Popa*, 1996). Large intermediate-depth events with magnitude M=6.5 occur two to five times per century. During the last century there were four large events: in 1940 (M=7.7), in 1977 (M=7.5), in 1986 (M=7.2) and in 1990 (M=6.9) which caused serious damages in the neighboring areas. The shallow seismicity in this area is much weaker.

Several seismic tomography studies have been previously performed in this region. The first studies investigating the three-dimensional velocity structure in the Vrancea area used the P-wave arrivals from teleseismic earthquakes recorded by the Romanian Seismic Network (*Fuchs et al.*, 1979*; Oncescu,* 1982; 1984*; Oncescu et al.,* 1984*; Koch,* 1985*)*. Later studies *(Wortel and Spakman,* 1992*; Lorenz et al.,* 1997, *Fan et al.,* 1998, *Popa et al.*, 2001*)* inverted for the velocity structure using P- and S-phase arrivals from local and regional events. Significant advances in the understanding of the deep seismic structure and seismicity in the Vrancea region were achieved as a result of the CALIXTO'99 experiment (*Wenzel et al.,* 1998). In particular, important results about the 3-D velocity structure in the mantle beneath the Vrancea area were obtained by *Martin et al.* (2005, 2006) from inversion of teleseismic data recorded within this experiment.

The aforementioned tomographic studies based on local, regional and teleseismic earthquake data put into evidence the high-velocity body located between 60 and 200 km depth, which sinks into the astenosphere almost vertically. This velocity pattern can be observed in the region where the Vrancea subcrustal seismic activity occurs. Studies of conversion waves coming from earthquakes that occurred in the Vrancea region and recorded at seismic stations in Romania (e.g., *Enescu et al.*, 1982) also suggest the presence of a quasi-vertical lithosphere fragment, located between depths of about 80 to 200 km. The teleseismic tomography by *Martin et al.* (2005) also evidenced a change in the orientation of the high-velocity body, from a NE-SW direction in the upper part to a N-S direction in the lower part. The P-wave velocity anomalies in this pattern are estimated to be at about 3 % with respect to the 1D reference model. Above this high velocity anomaly, the tomography results reveal the existence of a low-velocity structure. These findings have also been supported by analysis of seismic attenuation along rays from deep events beneath Vrancea performed by *Russo et al.* (2005).

The occurrence of the intermediate depth seismicity within the high seismic velocities in the upper mantle is interpreted as the transportation of cold and dense lithospheric material into the upper mantle. However, one major question that arises when trying to explain this process concerns the type of the descending material: is it a subducted oceanic lithosphere fragment or a delaminated continental material?

Early geodynamical models (e.g. *McKenzie*, 1970) suggested that the intermediate depth earthquakes beneath Romania occur in a relic oceanic slab sinking vertically within the mantle beneath the continental crust. Based on the existence of a gap in seismicity at a depth of 40-60 km (*Fuchs et al.*, 1979; *Constantinescu and Enescu*, 1984; *Oncescu*, 1984) and on the shape of seismic anomalies in aforementioned tomographic studies, many authors propose a mechanism of slab detachment beneath Vrancea. However, given the hypothesis of a complete detachment, it is hard to explain the relatively high strain rates inside the slab (probably associated with the strong slab pull forces). Moreover, a complete decoupling is not compatible with the gravitational instability mechanism. Therefore, a progressive decoupling along the Carpathian arc is proposed by some authors (e.g., *Wortel and Spakman*, 1993; *Matenco et al.*, 1997; *Sperner et al.*, 2001). One of the strongest arguments in favor of subduction of an oceanic slab beneath the Eastern Carpathians is the presence of a linear arc of Neogene volcanism within the hinterland (e.g. *Seghedi et al.,* 2004). This volcanic chain, which is comprised of both calc-alkaline and alkaline magmas, was active from the Middle Miocene to Quaternary time (13.4–0.2 Myr), and migrated successively from north to south (*Mason et al.*, 1998), even though major and trace element geochemistry of the calc-alkaline lavas suggest they are subduction-related (e.g., *Pecskay et al.*, 1995; *Mason et al.*, 1998, *Seghedi et al.,* 2004).

Delamination is one of alternatives to subduction mechanism of the lithosphere "recycling". This mechanism has been used for explaining the geodynamical processes in different areas after classical work on continental lithosphere sinking beneath the Colorado plateau by *Peter Bird* (1979). Delamination mechanism seems to be suitable for some cases of continent-continent collision (e.g., *Nelson*, 1991; *Houseman and Molnar*, 1997, *Ducea et al.,* 1998, *Gilbert et al.,* 2007) and, particularly, for the Vrancea region (e.g., *Knapp et al.,* 2005). It may also explain occurrence of mantle seismicity, as, for example, shown by *Seber et al.*, (1996) for the area of Alboran Sea. Delamination presumes a periodical localization of denser lithosphere material until it reaches a critical mass, at which point it forms a large drop that begins to fall down. For the Vrancea region, *Lorinczi and Hauseman* (2009) have recently modeled the Rayleigh-Taylor gravity instability due to higher density in the lithosphere in respect to the asthenosphere. They obtained a downgoing drop of the lithosphere material and estimated the strain-rates caused by this process which appear to be consistent with the focal mechanisms of the intermediate

seismicity beneath Vranchea. *Kay and Kay,* (1993), have proposed that the delamination process can be triggered by eclogitization of the lower crust matherial. *Sobolev et al.,* (2006) and *Babeyko et al.,* (2006), have modeled this situation for a collision area in Central Andes. They have shown that coupling of the continental crust in the collision areas may cause eclogitization of the lowermost crust, that results at accumulation of anomalously high density material in the bottom of the crust. This increases the gravity instability and favors forming falling "drops".

After presenting our tomographic results, in the Section of Discussion we will compare the subduction and delamination mechanisms for the Vrancea region in the light of the new findings.

3. Data and method of analysis

3.1. Data description

The earthquake data were provided by the CALIXTO'99 experiment and K2 network within the CRC461 programme of University of Karlsruhe (Germany) (*Wenzel et al.*, 1998; *Bonjer et al.*, 2000; *Bonjer and Rizescu*, 2000; *Bonjer et al.*, 2002) and Romanian Seismic Network (*Neagoe and Ionescu,* 2009). The data set consists of P- and S-wave arrival times of 994 local events (Figure 3A) that were recorded from 1982 to 2006. The earthquakes were selected by requiring a minimum of six P-wave arrivals with a clear onset per event, and an RMS smaller than 0.5 s. There are 687 intermediate-depth events and 307 crustal events that fulfilled this criterion. The distribution of temporary and permanent seismic stations that recorded the earthquakes is shown in Figure 3B. The temporary network was in use during the CALIXTO'99 experiment and consisted of 30 broad-band and 90 short-period stations, installed in a region of about 350 km in diameter and centered in the Vrancea area. There were 160 local events ($M_L \geq$ 2.0) that were recorded in a period of six months during CALIXTO'99. In 2006, the Romanian Seismic Network had about 120 stations in the area between 43.5-48º N latitude and 21-29º E longitude. Most of the stations are located in the Eastern and Southern Carpathians and are primarily designed to survey the Vrancea seismic region, at the Carpathians Arc Bend. The initial event locations were found using the HYPOPLUS program (*Oncescu et al.*, 1996), which is used by NIEP for routine earthquake locations (*Oncescu et al.*, 1999). The quality of the initial earthquake locations is relatively high, with a mean value of RMS travel time residuals below 0.5 s. To select data for the tomographic inversion we performed additional analysis to reject the outliers and events with less than 10 picks. The final dataset consists of 16199 arrival times from 653 events with 8529 P-wave and 7670 S-wave arrival times.

3.2. Inversion method

The 3D tomography inversion was performed using the LOTOS code which is freely available at www.ivan-art.com/science/LOTOS. The code is described in detail by *Koulakov* (2009). Here we present very briefly the main steps of the algorithm.

The input files for our calculations include the list of the stations with coordinates and elevations, and a catalogue of the arrival times from local earthquakes. The algorithm does not require any information about coordinates and origin times of the sources. However, using the preliminary locations of sources allows us to speed up the calculations. In addition, a starting 1D velocity model and a set of free parameters for different calculation steps should be defined.

The calculation begins with preliminary earthquake locations in a 1D velocity model. At this stage, the source coordinates and origin times are determined using a grid search method (*Koulakov and Sobolev*, 2006a). The method ascertains the maximum of a Goal Function (GF) that reflects the probability of the source location in the 3D space. The model travel times are computed using tabulated values calculated in the 1D velocity model at a preliminary stage. This makes the preliminary location step relatively fast and stable. The location of sources in the 1D model alternates iteratively with the optimization step for the 1D model, which is based on matrix inversion for the 1D velocities (Vp(z), Vs(z)), source coordinates and origin times.

After performing the preliminary locations and optimization for the 1D model, the main stage of the tomographic inversion begins. It consists of several steps that are performed sequentially and looped iteratively. In the first step, the sources are relocated in the 3D velocity model. The rays are traced using the bending method (*Koulakov*, 2009). In the first iteration, the relocation is performed in the 1D model, and in the following iterations it uses previously updated 3D models. The second step is parameterization grid construction. The LOTOS-09 code gives two possibilities for the parameterization: with cells and with nodes. Here we use only the node parameterization, which we found to be more robust. The main feature of the parameterization in the LOTOS code is the minimization of any effect of grid configuration upon the result. This is achieved by reducing the node spacing to values that we assume to be significantly smaller than the expected size of anomalies. Furthermore, we reduce the bias of the chosen grid configuration on the final tomographic images by repeating the inversion using grids with different basic orientations (e.g., 0°, 22°, 45°, and 67°) and averaging the results. The matrix inversion for P and S velocity and source parameters (dx, dy, dz and dt for each source) is performed using the LSQR method (*Page and Saunders*, 1982; *Van der Sluis and van der Vorst*, 1987). The inversion can also be performed for P velocity and the Vp/Vs ratio using the algorithm described in *Koulakov et al.* (2007). The amplitude and smoothness of the solution are controlled by two additional matrix blocks. The weights of these blocks play an important role in

tuning the resulting model. These parameters, as well as weights for source corrections and other free parameters, are estimated using synthetic modeling.

4. Results

4.1. 1D model optimization

Data processing started with preliminary source location and optimization for the 1D velocity model. To assess the robustness of this procedure, we performed a series of tests (Figure 4) using the observed and synthetic data. The 1D model that best explains the observed data was determined using different starting velocity models (Figure 4A). We experimented with different velocities and velocity gradients above and below Moho and used different thickness values for the high gradient layer, which represents the transition from the lower crust to the upper mantle. As an example, some of them are shown in Figure 4A by dotted lines. The RMS values of residuals for five models after their 1D optimizations are presented in Table 1. All models have significantly different starting values for P and S wave velocity in the crust. The resulting velocity distributions are closer to each other (especially for the S model); however for the P model the difference remains quite significant. Regarding the results related to the mantle, it is shown that the P velocity solution is less robust than that of the S velocity. In fact, for Model 1, the resulting distribution of P velocity concurs with the results obtained for other starting models only in the uppermost mantle depth (50-70 km depth). For the deeper layers the result remains close to the starting value. For the S model, the optimization provides similar results for significantly different starting models. It is surprising that for the S-wave velocity model the solution appears to be more robust than for the P-wave model.

Based on the analysis of the resulting velocity distributions and the RMS of residuals, we can conclude that the most probable 1D velocity distribution in the Vrancea region corresponds to Model 5, which is presented in Table 2. According to this model, the P and S velocities in the mantle are about 8.2-8.3 km/s and 4.8-4.9 km/s, respectively. These values are significantly higher than those used for routine locations of earthquakes in this area (7.94 – 8.17 km/s and 3.86 – 4.58 km/s for P and S models, respectively) and are closer to the values of the minimum 1D model determined using the VELEST inversion algorithm *(Kissling et al.*, 1995; *Popa et al.*, 2001).

The stability of the solution in the presence of random noise affecting the observed data was assessed by using the “odd/even” event test (e.g. *Koulakov et al.*, 2007). The test consists of carrying out independent inversions of two randomly selected data subsets (obtained, for

example, by selecting from the whole earthquake data set the odd and even numbers of events in the database). The results of the 3D inversions for this test are presented in Appendix 2. Here, we show the optimization results for the 1D velocity models (Figure 4B). The starting models for the subsets with odd and even events, and for the entire dataset, are the same and correspond to Model 5 in Figure 4A. It is shown in Figure 4B that the optimization results in all cases are similar. Only for the crustal layers, where slightly higher velocities are derived for the odd data subset, are differences found. This test shows that the chosen set of data does not affect significantly the stability of the 1D model optimization.

The stability and robustness of the 1D velocity optimization was also investigated using synthetic modeling. In Figure 4C, we present the optimization results for the checkerboard test. The 3D reconstruction of the checkerboard model will be discussed in Section 4.5. Here, we show the 1D optimization results based on two presumably incorrect starting velocity distributions. In the first case, the starting P and S velocities (violet lines) are lower than the "true" ones (red lines) by a constant value of 0.2 km/s. In the second case (green lines), the velocities are regularly higher by the same value. It is shown that for the crustal depth the optimizations provide values that are close to the "true" ones, while, for the lower part of the model, the velocity does not deviate from the starting values. This can be attributed to the fact that the majority of the sources are deep and the trade-off between focal depth, origin time and seismic velocities prevents us from obtaining stable solutions for absolute velocities. Again, as in the cases of measured data inversions, for the synthetic reconstructions we observe better stability for the S velocity optimization. It is important to note that in these two checkerboard analysis the RMS of residuals after optimization have similar values: 0.5005 s and 0.4988 s, respectively. The fact that considerable velocity variations cause very small changes of RMS explains the rather low stability for absolute velocity determination in this case. At the same time, it will be shown later that the relative 3D anomalies, which are based on different reference models, are reconstructed similarly. This shows a higher stability of relative anomaly determinations when compared to absolute values in this observation scheme.

4.2. 3D tomographic inversion

The LOTOS code allows us to perform the inversion in two schemes: for the Vp – Vs and Vp – Vp/Vs ratio. Performing the inversion for both schemes provides additional constraints for the relationship between the amplitudes of P and S anomalies. Note that in the former scheme we minimize the P and S residuals, while in the latter scheme we process the P and P-S differential residuals. This means that the solutions obtained for the S model using the two schemes are

independent, which provides additional information to verify the robustness of our results. In this section, we present the 3D velocity results using Vp-Vs inversion scheme which were selected as the main result of this study. The inversion results for Vp-Vp/Vs scheme are presented in Appendix 1. They include Vp, Vs anomalies and Vp/Vs ratio in horizontal and vertical sections (Figures A1-A3). Comparing the results derived independently using these two schemes provides a possibility to assess the robustness of the reported patterns.

In all cases the inversion was performed in five iterations, which was a compromise between calculation time and the quality of the solution (reducing the non-linear effect). Increasing the number of iterations would roughly be equivalent to decreasing the damping for an unchanged number of iterations. The RMS of residuals after the 1st and 5th iterations are shown in Table 3. In general, the Vp - Vp/Vs scheme leads to larger RMS than the Vp-Vs inversion. However, this does not mean that the former scheme provides a worse solution than the latter, when taking into account that the inversion for Vp-Vp/Vs ensures minimization of differential P-S residuals, while Vp-Vs scheme minimizes the P and S residuals that are accounted for in the reported RMS.

Figures 5 – 7 show the results for P and S anomalies in eight horizontal and two vertical sections that correspond to the Vp - Vs inversion scheme which are the main result of this study. The resulting locations of sources after five iterations of coupled inversion around each section are also shown. These anomalies and their possible interpretation will be discussed in detail in Section 5.

Any tomographic inversion guaranties obtaining some results, but just reporting the derived seismic structure without sufficient verification seems to be not adequate. We have performed dozens of different tests with real and synthetic data and some of them are presented in Appendices 2-5. It particular, it seems to us very important to explore the effect of starting 1D model on the resulting velocity anomalies (Appendix 2). The results of 1D model optimization (Section 4.1) shows that for some depth interval it does not provide stable solution. Does it affect the results of 3D inversion? Comparing the velocity anomalies in the main model (Figures 4, 5) and ones based on another reference model shows rather good correlation. This means that the reported velocity anomalies appear to be more robust than absolute values. A similar observation has been made by *Koulakov et al.* (2007). The effect of random noise, which is considerable in the used dataset, can be evaluated using independent inversion of two data subset (odd/even test). The results of this test which are discussed in Appendix 3 reveal the minimal size of trustworthy patterns provided by the existing dataset.

In this study we pay much attention to performing synthetic modeling which allows us to find optimal values of free parameters (e.g. damping), to evaluate the spatial resolution, and to

367 estimate the realistic amplitudes of the anomalies. When performing the synthetic tests we
368 simulate as close as possible realistic situations when neither location of sources, nor reference
369 1D model are known a-priori. In this case the synthetic modeling reveals conservative resolving
370 capacity of tomographic inversion, and it allows us to avoid over-interpreting some questionable
371 anomalies. In Appendix 4 we describe in details the conditions of performing the synthetic
372 modeling and show the results of 3D checkerboard test. One of the most important results of this
373 test is that it shows that we have sufficient vertical resolution to distinguish an anomalous body
374 below 65 km depth. Another synthetic test which is presented in Appendix 5 consists in
375 construction of a model which after consequent performing the forward modeling and inversion
376 enables the same structure as in the case of observed data. If the inversions with identical
377 parameters provide similar models for the cases of real and synthetic data, the synthetic model
378 may adequately represent the velocity distribution in the real Earth. In particular, this test is
379 important to evaluate realistic values of amplitudes of seismic anomalies. Based on a comparison
380 of synthetic and real images we can draw some important conclusions about the amplitudes and
381 shapes of anomalies, which are presented in the next section.
382

383 ## 5. Discussion of the resulting velocity patterns and interpretation

384 Figures 5 - 7 show the presence of a high velocity material in the depth interval of 60 to
385 180 km, which coincides with the distribution of active intermediate-depth seismicity. These
386 findings generally corroborate the results obtained in previous tomographic studies *(Wortel and*
387 *Spakman,* 1992*; Lorenz et al.,* 1997, *Martin et al.* 2005, 2006*)*. Our results are in qualitative
388 agreement with S-velocity model derived from inversion of surface waves by *Boschi et al.,*
389 (2009) who found a slow heterogeneity under the Carpathians, underlain by a fast one, with the
390 transition at ~100-150km depth. The tomography investigations using teleseismic data (*Wortel*
391 *and Spakman*, 2000; *Martin et al.*, 2006) pointed out a well-defined high-velocity body
392 extending down to a depth of about 400 km. Our results, obtained from the inversion of local
393 data, generally agree with the previous studies, showing, however, a better resolved geometry for
394 the crust and upper mantle down to about 200 km beneath the Vrancea seismic area. The velocity
395 anomalies in the crust are generally negative and continue beneath the Vrancea region down to a
396 depth of around 60 km, where very few seismic events are detected (Figure 7). In our study,
397 higher data quality and many different tests performed allow us to single out the most confident
398 features and to see the processes beneath Vrancea from another point of view. In the following,
399 we consider both the slab detachment and delamination models for the lithosphere recycling
400 beneath Vrancea.

In Figure 8A we present an interpretation cartoon for a subduction and slab detachment scenario beneath the Vrancea region, which is overlapped by our tomographic results in a vertical section. In our tomogram, the deep high-velocity body is clearly separated from the high-velocity Moesian block, which does not agree with the concept of current progressive decoupling (e.g., *Wortel and Spakman,* 1993; *Matenco et al.,* 1997; *Sperner et al.,* 2001). In the vertical section, we see that the distance between these high velocity bodies is about 50 km. Seismic activity inside the deep body indicates that it cannot be suspended in a steady state and that it should progressively move down. Let us consider an underestimated rate of sinking at 1 cm/year which is much slower than 2.5 cm/yr rate of pre-Oligocene convergence estimated by (*Roca et al.*, 1995). With a lower rate, the stresses would probably be too low to produce seismic activity. Dividing the 50 km gap between high velocity bodies to this rate, we can estimate that the detachment occurred about 5 Ma or less. If we associate this detachment with the closing of an oceanic basin, this brings us logically to a conclusion that before this age in Vrancea area there was an oceanic lithosphere. However, if an ocean-floored basin was consumed during the formation of the Eastern Carpathians, evidence for the former boundary between two distinct continental plates should have been recorded in both the surface geology (suture zone) and the underlying crustal structure. To date, no conclusive evidence has been found for such a recent (5Ma) crustal (and lithospheric) boundary. On the other hand, some authors argue that detachment does not need to occur immediately after subduction stops. For example *Van der Zedde and Wortel* (2001) show that due to a rather long transition zone of the lithosphere from the oceanic to continental type, there can be a delay of millions of years. However, according to (*Ellouz and Roca*, 1994; *Linzer et al.*, 1998), active shortening stopped at about 20 MA. It means more than 15 million years of delay between closing of the oceanic basin and detachment of the slab. At the same time, results of numerical modeling usually provide much shorter time of the break-off occurrence (e.g. *Buiter et al.,* 2002). Furthermore, this explanation presumes that the detached lithosphere is not of oceanic type, but mostly continental. The relatively low density of this detached block prevents fast sinking which is necessary for producing the observed high strain-rates.

Detailed comparison of the intermediate-depth seismicity with the shape of the high velocity body does not corroborate the idea of slab detachment. Indeed, intermediate seismicity in classical oceanic subduction zones is localized close to the upper surface of a slab. In some cases, it can form double seismic zones (e.g., *Nakajima et al.,* 2001), however, both earthquake planes are parallel to the slab upper interface. In the case of Vrancea, the deep seismicity begins at a depth of 60 km where we can still observe low velocity (in area with question mark in Figure 8A). Deeper, the cluster is traced down almost vertically. It passes throughout the central part of

436 the high velocity "slab", while in the classical subduction model it should be observed closer to
437 the upper (left in the presented section) border of the subducted lithosphere. Furthermore, the
438 large variety of focal mechanism solutions for Vrancea earthquakes and the complexity of the
439 compression and tension axes orientations (e.g., *Enescu and Enescu,* 1998) are also difficult to
440 explain using the framework of classical subduction. Based on the arguments presented in the
441 above paragraphs, we assume that the concept of subduction and slab detachment in the Vrancea
442 case contradicts some of the estimates and observations.
443 Delamination, as an alternative to subduction mechanism of the lithosphere "recycling"
444 was initially proposed by *Bird* (1979) and further developed by other authors (e.g. *Kay and Kay,*
445 1993, *Sobolev et al.,* 2006 and *Babeyko et al.,* 2006). According to some authors, the
446 delamination mechanism is suitable for the cases of the Vrancea region (e.g., *Knapp et al., 2005*).
447 A possibility of the two alternative mechanisms, slab detachment and delamination, is also
448 discussed in (*Russo et al.,* 2005) based on attenuation of seismic waves from deep events beneath
449 Vrancea.
450 Interpretation of our tomography results in terms of delamination mechanism is presented
451 in Figure 8B. This scenario can be supported by results of *Babeyko et al.* (2006) based on 2D
452 numerical modeling (Figure 24.4 in the referenced monograph). In this model, the crust consists
453 of two layers: these are felsic upper and mafic lower crust. At the initial step of compression, the
454 crust is laterally homogeneous and the lithosphere is slightly thinned in the central part of the
455 model. The compression causes maximal deformations in the central part of the model where the
456 lithosphere is weakest (e.g., *Lankreijer et al.,* 1997). This deformation leads to considerable
457 thickening of the crust (both felsic and mafic layers). Due to the deepening of the mafic material
458 and the changing of the P-T conditions, it is transformed to eclogite, which is much denser than
459 the underlying lithosphere. When a critical mass of the eclogitic lower crust is accumulated, it
460 forms a drop surrounded by unstable lithosphere material that begins to fall. According to
461 estimates presented by *Babeyko et al.* (2006), the sinking velocity of this drop is very high and
462 can reach several dozen centimeters per year. It is obvious that such a high speed can cause
463 abrupt changes in P-T conditions inside the lithospheric drop and very strong stresses that are
464 responsible for the active seismicity. The possibility cannot be excluded that such a fast process
465 leads to phase transitions of the remaining crustal material inside the delaminating drop, which is
466 associated with the release of fluids. In turn, these fluids might decrease the melting temperature
467 of the overlying rocks and may lead to the formation of volcanoes in the area similarly as in the
468 case of oceanic subduction. After delamination, the crust above the falling drop consists mostly
469 of a thick felsic part that can be expected with low seismic velocities. Our tomographic result
470 shows low velocities in the crust beneath Vrancea and seems to corroborate this idea. Also,

Sobolev et al. (2006) have shown that delamination leads to high topography, which is clearly seen in the Carpathians.

Inferences based on the work of *Babeyko et al.* (2006) must be made with caution, as the modeling exercise conducted by those authors is limited to 2D, while in the Vrancea area the general structures are 3D. The natural question when passing from 2D to 3D setup is whether these falling material forms in map view isometric "drops" or elongated "walls". 3D modeling of Rayleigh-Taylor gravity instability (e.g. *Lorinczi and Hauseman,* 2009) demonstrates the isometrical character of drops. Intuitively it is clear that elongated "walls" are unlikely. Indeed, in the case of a wet flat ceiling in a bathroom, the drops of water fall more or less chaotically and they are isometric. Even the existence of long beams on the ceiling does not change this feature: the drops are originated as isometric features located at some distances from each other along the beams.

The delamination process and slab detachment seem to be mutually exclusive mechanisms; their combination in the Vrancea region is not likely. The subduction process presumes a continuous penetration of high velocity material into the mantle, while the delamination mechanism is related to periodic falling of discrete "drops". The time of accumulation of critical mass of the eclogitic material according to the modeling results (*Babeyko, et al.,* 2006) is more than ten times longer than that of its falling. We expect that in Vrancea there is a chance to observe a rare process of drop falling, which lasts for a relatively short time when compared to the time of accumulation.

Saying about delamination in Vrancea we should draw parallels with other areas where similar mechanism has been proposed by other authors. Delamination of continental lithosphere is a geodynamic process that has been popular ever since a classic paper on the Colorado Plateau (*Bird,* 1979). There is a large body of literature on the Sierra Nevada batolith where ongoing aseismic delamination is proposed by *Ducea et al.,* (1998), *Gilbert et al.,* (2007) and many others. A comprehensive analysis of various data (seismicity, gravity, seismic attenuation and others) for the Alboran Sea in Western Mediterranean leads to the conclusion about active delamination of a piece of continental lithosphere (*Seber et al.,* 1996). Complex interaction of ongoing subduction and delamination of continental Brasilian lithosphere is proposed in Central Andes (e.g. *Kay and Kay,* 1993, *Sobolev et al.,* 2006). The image of the high velocity anomaly beneath the Vrancea region is somehow similar to the results obtained for the Pamir Hindu-Kush region (*Koulakov and Sobolev*, 2006b). We suppose that a similar delamination mechanism might take place there on a larger scale. In the Pamir Hindu-Kush region, a large high-velocity body in the upper mantle fits with the clusters of very active intermediate-depth seismicity (down to 300 km). This pattern is almost vertical and, in planar view, it is almost isometrical. The seismicity is

506 traced inside this body, not along its border, as presumed in the case of subduction. Furthermore,
507 the subduction concept presumes the sinking of a high velocity oceanic lithosphere that requires
508 the closing of an oceanic basin in the recent past. However, there is no geological evidence for
509 such a process in the Pamir Hindu-Kush region in the past 50 million years.
510 We suppose that delamination is one of the main mechanisms of lithosphere recycling in
511 areas of continent-continent collision. In the Alpine-Himalayan belt, the falling of the
512 delaminating drops may occur in any part of the collision zone. However, the time of
513 accumulation of the unstable material is much longer than the time of falling. Therefore, we now
514 have a chance to observe these drops only in two places: in Vrancea and Pamir-Hindu-Kush.
515 Two other areas in Asia where intermediate-depth seismicity can be observed, Zagros (Iran) and
516 Burma, are more likely ascribed to the classical subduction of oceanic plates.
517

518 # 6. Conclusions

519 The results presented in this study, obtained from the tomographic inversion of local data,
520 generally concur with the results of previous studies, showing however a more highly resolved
521 geometry for the crust and the upper mantle down to about 200 km beneath the Vrancea seismic
522 area. Taking into account the fact that seismic tomography is still an imperfect tool, the observed
523 correlation with the previous results is an informal argument for the robustness of the main
524 patterns derived independently by different authors based on different datasets.
525 The main resulting feature of the tomographic model derived in this study (as well as in
526 most previous studies) is a high velocity pattern located below a depth of 60 km, which generally
527 coincides with the distribution of intermediate-depth seismicity. Most of the previous studies
528 interpreted this anomaly as a detached part of an oceanic slab. We present several arguments that
529 contradict this model, such as:
530 - Taking into account the considerable descending speed of this high-velocity
531 "oceanic lithosphere" (at least 1 cm/year), the detachment occurred not earlier than
532 5 million years ago, which presumes closing of the oceanic basin at the same time.
533 However, there is no evidence of the existence of any oceanic basin in Vrancea in
534 the recent past.
535 - If this body is suspended and does not move down, no seismic activity would be
536 observed in such a steady-state system.
537 - The seismicity cluster passes through the central part of the high velocity body, and
538 is not located close to its upper surface, as presumed by subduction.

We propose an alternative concept of delamination, which can explain most of the existing facts. According to this concept, we currently observe a falling "drop" consisting of eclogitic lower crust material surrounded by untrained lithosphere material. This delamination occurs after a long stage of accumulation of denser eclogitic material in the bottom of the crust. These eclogites are the result of phase transition in the mafic layer due to the thickening of the crust. We propose that this process of accumulation and delamination of eclogitic material might take place in most zones of continent-continent collision. However, the active phase of the falling "drop", which is relatively short compared to the phase of accumulation, is currently observed only in few places (e.g., Hindu-Kush and Vrancea). We hypothesize that delamination, and not subduction, is the main mechanism of recycling the lithosphere material in the continent-continent collisional belts.

Acknowledgements

The earthquake data are provided by the CALIXTO'99 experiment and K2 network within the CRC461 programme of University of Karlsruhe (Germany) and the Romanian Seismic Network. The work of Ivan Koulakov is supported by the Russian Federation for Basic Researches (08-05-00276-a), Helmholtz Society and RFBR Joint Research Project 09-05-91321-SIG a, Multidisciplinary Projects SB RAS #21, SB-UrO-DVORAS #96, and Project ONZ RAS #7.4. The training stages of Bogdan Zaharia at GFZ - German Research Centre for Geosciences, Potsdam, Germany were funded by the CORINT Project no. 49/2006 of the Romania Ministry of Education and Research and NATO SfP project no. 981881. We are grateful to the Editor, Thorsten Becker, for rigorous and constructive criticism, as well as to Lapo Boschi and an anonymous reviewer for their critical remarks which helped us to improve the paper.

Appendices:

Appendix 1. Inversion for Vp-Vp/Vs scheme

Besides the main results which were obtained using the Vp-Vs inversion scheme shown in Section 4.2 (Figures 5-7) we present the results computed independently according to Vp-Vp/Vs scheme. The values of the Vp/Vs ratio in horizontal sections derived by inverting the Vp and Vp/Vs ratio are presented in Figure A1. Values of Vp, Vs and Vp/Vs in a vertical section A-A' are shown in Figure A2. Note that in this case, values of Vs are computed by dividing the resulting Vp by Vp/Vs. Distributions of Vs derived from Vp-Vs and Vp-Vp/Vs schemes are compared in two horizontal sections in Figure A3. The results obtained using the two schemes show similar features for the S velocity anomaly, however only at a qualitative level. Although we performed calculations for a dozen sets of free parameters (amplitude damping, smoothing and weighting balance between Vp and Vp/Vs ratio) in each case, we could not achieve an ideal correlation of the amplitudes and shapes of the anomalies. The difference between the results obtained using the two inversion schemes could be related to fundamental differences in the two approaches, namely, minimizing the P and S residuals and the differential P-S residuals, respectively.

Appendix 2. Effect of the starting velocity model upon the resulting 3D velocity anomalies

In Section 4.1 we discussed the problem of the relatively low stability of the 1D reference model optimization. It is important to check how the uncertainty of absolute velocity determination in the starting model for the 3D inversion affects the relative velocity anomalies. To answer this question, we have performed the full iterative inversion with the same free parameters as for the model presented in Figures 5-7, but based on a different reference model (Model 1, blue line in Figure 4A). The resulting patterns in this case, as shown in Figure A4, are almost identical to those in the main model (Figures 5-7), and the RMS value, which is reported in Table 3, is not considerably different. It shows that the relative perturbations are much more robust than the absolute velocity values. A similar observation has been made by *Koulakov et al.* (2007).

Appendix 3. Odd/Even test

Study of the posterior residuals after the inversion shows that the dataset used in this study is rather noisy. The contribution of the random noise upon the final result can be estimated using the "odd/even test" (see also Section 4.1). The inversion procedure is identical to the one used to derive the major results (Figures 5-7) and includes the step of 1D model optimization. The resulting 1D distributions for the odd and even data subsets are shown in Figure 4B. It can be seen that despite some discrepancies in the models in the crust, for the major parts the curves appear similar. The results of 3D P and S velocity reconstructions for the two subsets are presented in horizontal and vertical sections in Figures A5 and A6. Looking at these images, one can immediately identify which anomalies are trustworthy and which ones are caused by noise. For example, at a depth of 30 km, the patterns that are smaller than 30 km are probably not robust. At the same time, a large negative anomaly in the central part of the study area seems to be reliable. Most importantly, the positive anomaly patterns in lowest sections seem to be robust in both shape and amplitude. Comparing these test results with the main results presented in Section 4.2 shows that halving the dataset also has some effect upon the results and makes the solution less stable.

Appendix 4. Checkerboard test

To assess the spatial resolution of the model we performed a synthetic test using the standard checkerboard input model with alternating positive and negative velocity variation patterns. When performing the synthetic modeling, it is important to carry out the simulations in a manner as close as possible to observed data processing. In particular, it is necessary to adhere to several rules:

1. The parameterization of the synthetic model used for the forward calculation of the travel times should be different from that used during the inversion. For example, defining the synthetic patterns in the same parameterization nodes/blocks used for inversion is not appropriate as it fixes the periodicity of anomalies in the most convenient way for the algorithm. In reality, such predefinition of structural periodicity is, of course, not available.
2. The concept of the optimal 1D model used for computing synthetic times should be substituted with a more realistic acceptance of starting from an approximated 1D model. It was showed that in terms of relative variation of velocity, the results are not affected by this choice (*Koulakov*, 2009).

3. After computing the synthetic travel times, the coordinates and origin times of sources should not be used in the inversion procedure. In fact, ideally, the synthetic data file should not contain any information about the sources, and their location should begin from the initial stage. However, one can also begin the inversion procedure using the rough source locations in the 1D velocity model because they are generally different from the "true" 3D locations, thus respecting the rule.
4. When reconstructing the synthetic model, all parameters and procedural steps should be absolutely identical to observed data processing.

The synthetic testing performed according to these rules allows not only the assessment of the resolution of the model, but also estimation of optimal values of the free inversion parameters (e.g., amplitude damping and smoothing), which can be then used to enhance the real data results. For this study, we inverted synthetic and observed data in turn several times to obtain the best values for the parameters.

The synthetic travel times are computed by bending ray tracing through the synthetic model, which is represented by alternating positive and negative velocity anomalies summed up with the 1D velocity model indicated in Figure 4C by a red line. Laterally, the size of the patterns is 30 km along the latitude and longitude. In the vertical direction the change of sign is defined at 65 km and 140 km depth. The configuration of the model is shown in Figure A7 with thin black lines in map view and in vertical sections. The amplitudes of the anomalies were ±5% and ±7% for P and S models, respectively. The computed synthetic times were perturbed with random noise that have a realistic distribution histogram constructed previously from analyses of many different actual datasets. This histogram is slightly biased with respect to the traditionally used normal Gaussian distribution. The average amplitude of noise was defined at 0.1 s and 0.15 s for P and S synthetic travel time data, respectively.

The reconstruction begins with the relocation of the sources and the optimization of the 1D velocity model. We have performed the reconstructions with two starting models, which are indicated in Figure 4C by violet and green lines. Here, we present the result that corresponds to the violet lines; however, for the other case, the obtained anomalies are identical. This shows again that the tomography inversion for this observation scheme provides the relative anomalies more robustly than absolute velocities, which should be interpreted carefully. The results of reconstructed P and S anomalies in the checkerboard tests are shown in Figure A7 in map view at depths between 30 and 110 km and in two vertical sections. It can be seen that in the upper section the periodic anomalies are reconstructed in most parts of the study area, while for the deeper layers the anomalies are reconstructed only in the central part where earthquakes occur.

We detect some diagonal smearing that should be taken into account when real data results are interpreted. In vertical sections, both P and S models demonstrate a rather robust reconstruction of the level at 65 km where checkerboard anomalies change sign. This seems to be important for considering the real data results where a change of sign also takes place at this depth.

Appendix 5. Reconstruction of realistic patterns

The result of seismic tomography inversion is like a photograph taken by a camera with a blurred and deformed lens, which biases the shapes and "colors" (amplitudes) of the true images. Therefore, it appears to be inadequate to report the quantitative parameters obtained after inversion of observed data as real data. We propose a test that allows for the investigation of the properties of the "camera" (inversion algorithm) and to retrieve information about probabilistic shapes and amplitudes of velocity anomalies on Earth. Furthermore, this test allows us to find the optimal values of free parameters (e.g., damping) used for inversion.

The purpose of this test is to build a synthetic model, which, after performing forward and inverse modeling, reproduces similar patterns as in the case of observed data inversion. Note that the inverse procedure (tomography + source location) should be performed absolutely identically and with the same free parameters as in the case of observed data. The initial locations of sources and "true" reference model should be "forgotten". Furthermore, after computing synthetic travel times, a random noise should be added, and its level is defined to provide the similar variance reduction, as in reality. When the inversion resembles the retrieved models in both the real and synthetic cases, the synthetic model may adequately reflect the structures on the real Earth. However, we admit that this procedure is theoretically non-unique and several models may lead to similar reconstructions. For example, such non-uniqueness due to vertical smearing was shown with two models for the Toba area, N. Sumatra (*Koulakov et al.*, 2009). This modeling allows us to investigate this effect and take it into account.

The synthetic model with realistic patterns for P wave velocity anomalies is shown in horizontal and vertical sections in Figures A8-A9. For the S model, the shape of patterns remained the same, but the amplitudes were 20-30% higher. The anomalies are defined in prisms that may have a complex shape when seen in map view and remain unchanged within a fixed depth interval. The prisms are defined in the depth ranges indicated in Figure A8, except for one deep high velocity anomaly, which is defined from 100 to 200 km. We performed several trials testing the, shapes and amplitudes of the synthetic patterns. The final model, which is presented in Figures A8 and A9, is quite similar to the actual anomalies shown in Figures 5 and 7.

696 **References**

697 Aki, K. (1977), Three-dimensional seismic velocity anomalies in the lithosphere, *J. Geophys., 43*,
698 235-242, 1977.

699 Babeyko, A.Y., Sobolev, S.V., Vietor, T, Trumbull., R.B. and Oncken, O (2006), Weakening of
700 the Upper Plate during Tectonic Shortening: Thermo-Mechanical Causes and
701 Consequences. In: Oncken O et al. (eds) The Andes – Active Subduction Orogeny.
702 ***Frontiers in Earth Sciences***, 1, Springer, 495-512, 2006

703 Badescu, D. (2005), The Evolution of the Tectono-stratigraphy of the Eastern Carpathians during
704 Mesozoic and Neogene Times. *Editura Economică*, Bucharest, 308 (in Romanian).

705 Bird, P. (1979), Continental delamination and the Colorado Plateau, J. Geophys. Res., **84**, 7561-7571.

706 Bonjer, K.-P. and M. Rizescu (2000), Data Release 1996-1999 of the Vrancea K2 Seismic
707 Network. Six CD's with evt-files and KMI v1-,v2-, v3-files. Karlsruhe-Bucharest, July 15.

708 Bonjer, K.-P., M.C. Oncescu, M. Rizescu, D. Enescu, L. Driad, M. Radulian, C. Ionescu, T.
709 Moldoveanu (2000), Source- and site-parameters of the April 28, 1999 intermediate depth
710 Vrancea earthquake: First results from the new K2 network in Romania, XXVII *General*
711 *Assembly of the European Seismological Commission, Lisbon, Portugal, Book of Abstracts*
712 *and Papers, SSA-2-13-O*, 53.

713 Bonjer, K.-P., M. Rizescu, and B. Grecu (2002), Data Release 2000-2001 of the Vrancea K2 Seismic
714 Network. Two CD's (evt-files). Bucharest- Karlsruhe, October 24.

715 Boschi, L., B. Fry, G. Ekstr¨om, and D. Giardini (2009), The Mediterranean upper mantle as seen by
716 surface waves, Surveys in Geophysics, 30, 463–501, doi:10.1007/s10712-009-9066-2.

717 Buiter S.J.H, R.Govers and M.J.R.Wortel (2002), Two-dimensional simulations of surface
718 deformations caused by slab detachment, Tectonophysics, 354, 195-210.

719 Burchfield, B.C. (1976), Geology of Romania. *Geol. Soc. Am., Spec. Pap. 158*, 82 .

720 Constantinescu, L., and D. Enescu (1984), A tentative approach to possibly explaining the
721 occurrence of the Vrancea earthquakes, *Rev. Roum. Géol., Géophys., Géogr., Géophysique,*
722 *28*, 19-32.

723 Csontos, L., A. Voros (2004), Mesozoic plate tectonic reconstruction of the Carpathian region,
724 *Palaeogeography, Palaeoclimatology, Palaeoecology 210*, 1–56.

725 Csontos, L. (1995), Tertiary tectonic evolution of the Intra-Carpathian area: a review. *Acta*
726 *Vulcanol. 7* (2), 1-13.

727 Carminati, E., M. J. R Wortel, W. Spakman, & R. Sabadini (1998), The role of slab detachment
728 processes in the opening of the western–central Mediterranean basins: some geological and
729 geophysical evidence, *Earth Planet. Sci. Lett. 160*, 651–665.

730 Ducea, M. N., and Saleeby, J. B. (1998), A case for delamination of the deep batholithic crust beneath the
731 Sierra Nevada, California. *International Geology Review*, 40 (1), pp. 78-93.

732 Enescu, D., I. Cornea, Fl. Radulescu, V. Raileanu and A. Pompilian (1982), Seismological data
733 on deep structure of Vrancea region, *Rev. Roum. Géol., Géophys., Géogr., Géophysique, 26*,
734 29-36.
735 Enescu, D., and B.D. Enescu (1998), Seismotectonic model regarding the genesis and the
736 occurrence of Vrancea (Romania) earthquakes, Romanian Reports in Physics, 50(1-2), 97-
737 122.
738 Evans, J.R. & U. Achauer (1993), Teleseismic velocity tomography using the ACH method:
739 Theory and application to continental-scale studies, in: *Iyer, H.M. and Hirahara, K.,*
740 *Seismic tomography: Theory and practice*, Chapman & Hall, London, 319-360.
741 Ellouz, N., and E. Roca (1994), Palinspastic reconstructions of the Carpathians and adjacent
742 areas since the Cretaceous: A quantitative approach, in *Peri-Tethyan Platforms, Technip,*
743 edited by F. Roure, *Paris*, 51–78.
744 Fan, G., T.C Wallace and D. Zhao (1998), Tomographic imaging of deep velocity structure
745 beneath the Eastern and Southern Carpathians, Romania: Implications for continental
746 collision. *J. Geophys. Res., 103*, 2705-2724.
747 Fuchs, K., K.P Bonjer, G. Bock, I. Cornea, C. Radu, D. Enescu, D. Jianu, A. Nourescu, G.
748 Merkler, T. Moldoveanu, G. Tudorache (1979), The Romanian earthquake of March 4,
749 1979. II. Aftershocks and migration of seismic activity. *Tectonophysics, 53*, 225-247.
750 Gilbert H., C. Jones, T. J. Owens, and G. Zandt (2007), Imaging Sierra Nevada lithosphere sinking, *Eos*
751 *Trans. AGU, 88*(21), p. 225-229.
752 Houseman, G.A. and P. Molnar (1997), Gravitational (Rayleigh-Taylor) instability of a layer
753 with non-linear viscosity and convective thinning of continental lithosphere, *Geophysical*
754 *Journal International, 128*, 125-150.
755 Kay RW, and Kay SM (1993) Delamination and delamination magmatism. Tectonophysics
756 219:177–189
757 Kissling, E., H. Kradolfer, L. Maurer (1995), VELEST user's guide short introduction, Techn.
758 Rep., Institute of Geophysics, ETH, Zurich.
759 Knapp, J. H., C. C. Knapp, V. Raileanu, L. Matenco, V. Mocanu, C. Dinu (2005), Crustal
760 constraints on the origin of mantle seismicity in the Vrancea Zone, Romania: The case for
761 active continental lithospheric delamination, *Tectonophysics 410*, 311 –323.
762 Koch, M. (1985), Nonlinear inversion of local seismic travel times for the simultaneous
763 determination of the 3D-velocity structure and hypocentres-application to the seismic zone
764 Vrancea, *J. Geophys. 56*, 160-173.
765 Koulakov, I., and S. Sobolev (2006a), Moho depth and three-dimensional P and S structure of
766 the crust and uppermost mantle in the Eastern Mediterranean and Middle East derived from

767 tomographic inversion of local ISC data. *Geophysical Journal International, Vol. 164*, issue
768 1, 218-235.
769 Koulakov I. and S.V. Sobolev (2006b), A Tomographic Image of Indian Lithosphere Break-off
770 beneath the Pamir Hindukush Region. *Geophys. Journ. Int., 164, p. 425-440.*
771 Koulakov, I., M. Bohm, G. Asch, B. Luehr, A. Manzanares, K. Brotopuspito, P. Fauzi, M.
772 Purbawinata, N. Puspito, A. Ratdomopurbo, H. Kopp, W. Rabbel, and E. Shevkunova
773 (2007), P and S velocity structure of the crust and the upper mantle beneath Central Java
774 from local tomography inversion, *J. Geophys. Res., 112*, B08310,
775 doi:10.1029/2006JB004712.
776 Koulakov I. (2009), LOTOS code for local earthquake tomographic inversion. Benchmarks for
777 testing tomographic algorithms, *BSSA, Vol. 99*, No. 1, pp. doi: 10.1785/0120080013.
778 Lankreijer A., V. Mocanu, S.A.P.L. Cloetingh (1997), Lateral variations in lithosphere strength
779 in the Romanian Carpathians: Constraints on basin evolution, *Tectonophysics 272*, 269-290.
780 Linzer, H.G., W. Frisch, P. Zweigel, R. Girbacea, H.P. Hann, F. Moser (1998), Kinematic
781 evolution of the Romanian Carpathians, *Tectonophysics 297*, 133-156.
782 Lorenz, F.P., B. Sperner, M. Popa, F. Wenzel (1997), New insights of the compressional-wave
783 velocity structure in the Vrancea subduction zone from teleseismic relative travel-time
784 residuals, *PANCARDI Workshop*, Krakow (Poland), Oct. 20-26.
785 Lorenz, F.P., M. Martin, B. Sperner, F. Wenzel, M. Popa (1997), Teleseismic travel-time tomography of
786 the compressional-wave velocity structure in the Vrancea zone, Romania, *EOS Trans. AGU vol. 78*,
787 nr. 46. supl. F497.
788 Lorinczi, P., and G.A. Houseman, (2009). Lithospheric gravitational instability beneath the Southeast
789 Carpathians, Tectonophysics, v. 474, iss. 1-2, p. 322-336, doi:10.1016/j.tecto.2008.05.024
790 Martin, M., J. R. R Ritter and the CALIXTO working group (2005), High-resolution teleseismic
791 body-wave tomography beneath SE Romania - I. Implications for three-dimensional versus
792 one-dimensional crustal correction strategies with a new crustal velocity model, *Geophys. J.*
793 *Int., Vol. 162*, Issue 46, 448-460.
794 Martin, M., F. Wenzel and the CALIXTO working group (2006), High-resolution teleseismic
795 body wave tomography beneath SE-Romania – II. Imaging of a slab detachment scenario,
796 *Geophys. J. Int. 164*, 579–595.
797 Matenco, L., R. Zoetemeijer, S. Cloetingh, C. Dinu (1997), Lateral variations in mechanical
798 properties of the Romanian external Carpathians: inferences of flexure and gravity
799 modeling, *Tectonophysics 282*, 147-166.
800 Mason, P. R. D., I. Seghedi, A. Szakacs, H. Downes (1998), Magmatic constraints on
801 geodynamic models of subduction in the East Carpathians, Romania, *Tectonophysics 297*,
802 157-176.

803 Neagoe, C. and C. Ionescu (2009), Toward a dense real – time seismic network in Romania,
804 *Romanian Reports in Physics* (accepted 2009).
805 Nakajima, J., T. Matsuzawa, A. Hasegawa & D. Zhao (2001), Threedimensional structure of Vp,
806 Vs, and Vp/Vs beneath northeastern Japan: implications for arc magmatism and fluids, *J.*
807 *geophys. Res., 106***,** 21 843–21 857.
808 Nelson, K.D., (1991), A unified view of craton evolution motivated by recent deep seismic
809 reflection and refraction results, *Geophysical Journal International 105* (1), 25– 35.
810 Oncescu, M. C. (1982), Velocity structure of the Vrancea zone (Romania), *Tectonophysics 90*,
811 133-143.
812 Oncescu, M .C., (1984), Deep structure of Vrancea region, Romania, inferred from simultaneous
813 inversion for hypocenters and 3-D velocity structure, *Ann. Geophysicae, 2*, 23-28.
814 Oncescu, M. C., V. Burlacu, M. Anghel and V. Smalbergher (1984), Three dimensional P-wave
815 velocity image under the Carpathian Arc, *Tectonophysics, 106*, 305-319.
816 Oncescu, M. C., M. Rizescu and K. P. Bonjer (1996), SAPS - A completely automated and
817 networked seismological acquisition and processing system, *Computer & Geosciences, 22*,
818 89-97.
819 Oncescu, M. C., V. Marza, M. Rizescu, M. Popa (1999), The Romanian earthquakes catalogue
820 between 984-1997. In: *Vrancea Earthquakes: Tectonics, Hazard and Risk Mitigation*,
821 edited by F. Wenzel, and D. Lungu, Kluwer Academic Publishers, pp. 43-47.
822 Paige, C. C., and M.A. Saunders, (1982), LSQR: An algorithm for sparse linear equations and
823 sparse least squares, *ACM trans. Math. Soft., 8*, 43-71.
824 Popa, M., E. Kissling, M. Radulian, K. P. Bonjer, D. Enescu, S. Dragan, and the CALIXTO
825 Research Group (2001), Local source tomography using body waves to deduce a minimum
826 1D velocity model for the Vrancea (Romania) zone, *Romanian Reports in Physics, 53*, 519-
827 536.
828 Popa, M., M. Radulian, B. Grecu, E. Popescu, and A. O. Placinta (2005), Attenuation in south-
829 eastern Carpathians area: result of upper mantle inhomogeneity, *Tectonophysics 410*, 235–
830 249.
831 Pecskay, Z., O. Edelstein, I. Seghedi, A. Szakacs, M. Kovacs, M. Crihan and M. Bernad, M.,
832 (1995), K-Ar datings of Neogene-Quaternary calc-alkaline volcanic rocks in Romania,
833 *Acta Vulcanologica, v.7*, 53-62.
834 Radulian M., M. Popa (1996), Scaling of the source parameters for the Vrancea intermediate
835 depth earthquakes, *Tectonophysics, 261*, 67-81.
836 Radulian M., M. Popa, O. F. Cărbunar, M. Rogozea (2008), Seismicity patterns in Vrancea and
837 predictive features, *Acta Geodaetica et Geophysica Hungarica 43*, 163-173.

838 Ratschbacher, L., O. Merle, Ph. Davy, P. Cobbold (1991), Lateral extrusion in the Eastern Alps,
839 part I: boundary conditions and experiments scaled for gravity, *Tectonics 10*, 245–256.
840 Roca, E., G. Bessereau, E. Jawor, M. Kotarba, F. Roure (1995), Pre-Neogene evolution of the
841 Western Carpathians: constraints from the Bochnia-Tatra Mountains section (Polish
842 Western Carpathians), *Tectonics 14* (4), 855-873.
843 Roure, F., E. Roca and W. Sassi (1993), The Neogene evolution of the outer Carpathian flysch
844 units (Poland, Ukraine and Romania): kinematics of a foreland. *Sedimentary Geology, 86*,
845 177-201.
846 Russo R.M., V. Mocanu, M. Radulian, M. Popa and K.-P. Bonjer (2005), Seismic attenuation in the
847 Carpathian bend zone and surroundings, *Earth and Planetary Science Letters* **237** pp. 695–709.
848 Schellart, W. P. and G. S. Lister (2004), Tectonic models for the formation of arc-shaped
849 convergent zones and backarc basins, in *Orogenic Curvature: Integrating Paleomagnetic*
850 *and Structural Analyses*, edited by A. J. Sussman and A. B. Weil, Spec. Pap. Geol. Soc.
851 Am., 383, 237– 258.
852 Seber, D., M. Barazangi, A. Ibenbrahim, A. Demnati (1996), Geophysical evidence for
853 lithospheric delamination beneath the Alboran Sea and Rif–Betic mountains, *Nature 379*,
854 785–790.
855 Seghedi I, Downes H, Szakacs A, Mason P R D, Thirlwall M F, Rosu E, Pecskay Z, Marton E & Panaiotu
856 C. (2004). Neogene-Quaternary magmatism and geodynamics in the Carpathian-Pannonian region:
857 a synthesis. Lithos, 72, 117-146.
858 Sobolev, S.V., Babeyko, A.Y., Koulakov, I. and O. Oncken, (2006). Mechanism of the Andean
859 orogeny: insight from the numerical modeling, In: Oncken O et al. (eds) The Andes –
860 Active Subduction Orogeny. ***Frontiers in Earth Sciences***, 1, Springer, 513-535.
861 Sperner, B., F. Lorenz, K. Bonjer, S. Hettel, B. Muller, F. Wenzel (2001), Slab break-off - abrupt
862 cut or gradual detachment? New insights from the Vrancea region (SE Carpathians,
863 Romania), *Terra Nova, 13*, 3, 172-179.
864 Sperner, B., D. Ioane, R. J. Lillie (2004), Slab behaviour and its surface expression: new insights
865 from gravity modelling in the SE Carpathians, *Tectonophysics, 382*, 51-84.
866 Van der Sluis, A., and H. A. van der Vorst (1987), Numerical solution of large, sparse linear
867 algebraic systems arising from tomographic problems, in: *Seismic tomography*, edited by
868 G.Nolet, pp. 49-83, Reidel, Dortrecht.
869 van de Zedde, D.M.A., and Wortel, M.J.R., (2001), Shallow slab detachment as a transient
870 source of heat at midlithospheric depths, Tectonics, v. 20, p. 868–882.

871 Wenzel, F., U. Achauer, D. Enescu, E. Kissling, R. Russo, V. Mocanu, G. Mussachio (1998),
872 The final stage of plate detachment; International tomographic experiment in Romania
873 aims to a high-resolution snapshot of this process, *EOS, 79: 589*, 592-594.
874 Wenzel F., F. P. Lorentz, B. Sperner, M. Oncescu (1999), in *Vrancea Earthquakes: Tectonics,*
875 *Hazard and Risk Mitigation, edited by* F. Wenzel, O. Novak and D. Lungu, Kluwer
876 Academic Publishers, Dodrecht, The Netherlands, 15-25.
877 Wortel, M. J. R. and W. Spakman (1992), Structure and dynamics of subducted lithosphere in
878 the Mediterranean region, *Proc. K. Ned. Akad. Wet. 95*, 325-347.
879 Wortel, M. J. R. and W. Spakman (1993), The dynamic evolution of the Apenninic-Calabrian,
880 Hellenic and Carpathian arcs: a unifying approach, *Terra Nova 5* (Abstr. Suppl.), 97.
881 Wortel, R. and W. Spakman (2000), Subduction and slab detachment in the Mediterranean –
882 Carpathian region, *Science, 290*, 1910-1917.
883

884

885 # Figure Captions

886 Figure 1. Main tectonic elements in Carpathian – Mediteranean region. The rectangle marks the
887 area of interest for this study. Abbreviations: IZ – Ivrea Zone, MP – Moesian Platform,
888 NAP – North Anatolian Fault, PB – Pannonian Basin, TB – Transylvania Basin, VR –
889 Vrancea.

890 Figure2. Southeastern Carpathian arc bend tectonical map (modified after *Badescu*, 2005).

891 Figure 3. Data used in this study. A.) Earthquakes distribution. Red and black dots show
892 intermediate-depth and crustal events, respectively. B.) Seismic stations: blue for
893 temporary network from CALIXTO and red for stations which are sending data to RO-
894 NDC.

895 Figure 4. Optimization of the 1D model for observed and synthetic data. A.) Optimization results
896 with observed data and different starting 1D models. Different colors indicate different
897 models; dotted lines are the starting models; bold lines of corresponding colors are the
898 optimization results. B.) optimization results for halved data subsets in the odd/even test.
899 C.) Optimization results for synthetic data in the checkerboard test presented in Appendix
900 4.

901 Figure 5. Horizontal sections of P velocity anomalies, in percent with respect to the optimized
902 1D velocity model, resulted from from the "Vp – Vs" inversion scheme. Dots depict the
903 relocated sources around the corresponding depth levels. Locations of profile presented
904 in Figure 7 are shown in section at 10 km depth.

905 Figure 6. Same as Figure 5, but for the S velocity anomalies.

906 Figure 7. P and S velocity anomalies derived from the "Vp – Vs" inversion scheme in two
907 vertical sections. Locations of the profiles are indicated in Figures 5 and 6. Dots depict
908 the relocated sources at distances of less than 40 km from the profile.

909 Figure 8. Interpretation cartoons based on the concept of subduction and slab detachment (Plot
910 A), and delamination (Plot B). Background is the velocity distribution and events resulted
911 from the tomographic inversion (P anomalies, Section A-A'), same as in Figure 7.

912 Figure A1. Vp/Vs ratio in horizontal sections derived from the "Vp - Vp/Vs" inversion scheme.
913 Dots depict the relocated sources around the corresponding depth levels.

914 Figure A2. P and S velocity anomalies and Vp/Vs ratio derived from the "Vp - Vp/Vs" inversion
915 scheme in the vertical section A-A' shown in Figure 5. Dots depict the relocated sources
916 at distances of less than 40 km from the profile.

Figure A3. S velocity anomalies obtained using the inversion schemes for Vp - Vp/Vs (upper row) and for Vp-Vs (lower row) in two horizontal sections. Dots depict the relocated sources around the sections.

Figure A4. P and S velocity anomalies from Vp-Vs inversion based on another reference model. Dots depict the relocated sources around the sections.

Figure A5. Odd-even test. Results for two halved subsets are presented for P and S anomalies in three horizontal sections. Dots depict the relocated sources around the sections.

Figure A6. Same as Figure A5, but presented in a vertical section. Location of the section is indicated in Figure A5.

Figure A7. Checkerboard test performed according to Vp-Vs scheme in two horizontal sections (upper row) and two vertical sections (lower row). Initial synthetic patterns are highlighted with thin black lines. Locations of the profiles are indicated in all maps. Relocated sources are shown with black dots.

Figure A8. Synthetic test aimed at reproducing the results of the real experiment. Only results for P velocity modeling are shown in horizontal sections. Synthetic model defined in 3D prisms is shown in the upper row. Values of anomalies are indicated by nu anomalies; depth diapason of prism definition is given above each plot. Lower row shows reconstruction results for P velocity anomalies and source locations (black dots).

Figure A9. Same test as in Figure A8, but shown in two vertical sections A-A’ and B-B’ with locations indicated in the upper maps in Figure A8. Upper row represents P synthetic model; lower row is the reconstruction results for P velocity anomalies and source locations (black dots).

941 **Tables**

942

943

Table 1. Values of the RMS after optimization for the 1D velocity distribution with different starting models	
Starting model	RMS of residuals, s
Model 1	0.5339
Model 2	0.5131
Model 3	0.5021
Model 4	0.4988
Model 5	0.4968

944

Table 2. P and S velocities in the reference 1D model after optimization (Model 5)		
depth, km	Vp, km/s	Vs, km/s
0	5.51	3.18
10	5.68	3.20
20	6.18	3.63
30	6.67	3.72
40	7.02	3.98
50	7.89	4.54
60	8.29	4.76
70	8.32	4.83
90	8.28	4.86
110	8.32	4.90
130	8.38	4.88
150	8.37	4.86
170	8.34	4.85
190	8.33	4.84
210	8.32	4.83
220	8.31	4.83

945

946

Table 3. Values of RMS of P and S residuals in 1st and 5th iterations in cases of different starting models and inversion schemes

Model description:	RMS of P residuals, 1 iteration, seconds	RMS of S residuals, 1 iteration, seconds	RMS of P residuals, 5 iteration, seconds	RMS of S residuals, 5 iteration, seconds
Ref model 5; Vp-Vs scheme	0.3637	0.6214	0.2037	0.3301
Ref model 1; Vp-Vs scheme	0.3686	0.6278	0.2113	0.3362
Ref model 5; Vp-Vp/Vs scheme	0.3637	0.6214	0.2090	0.3672

947

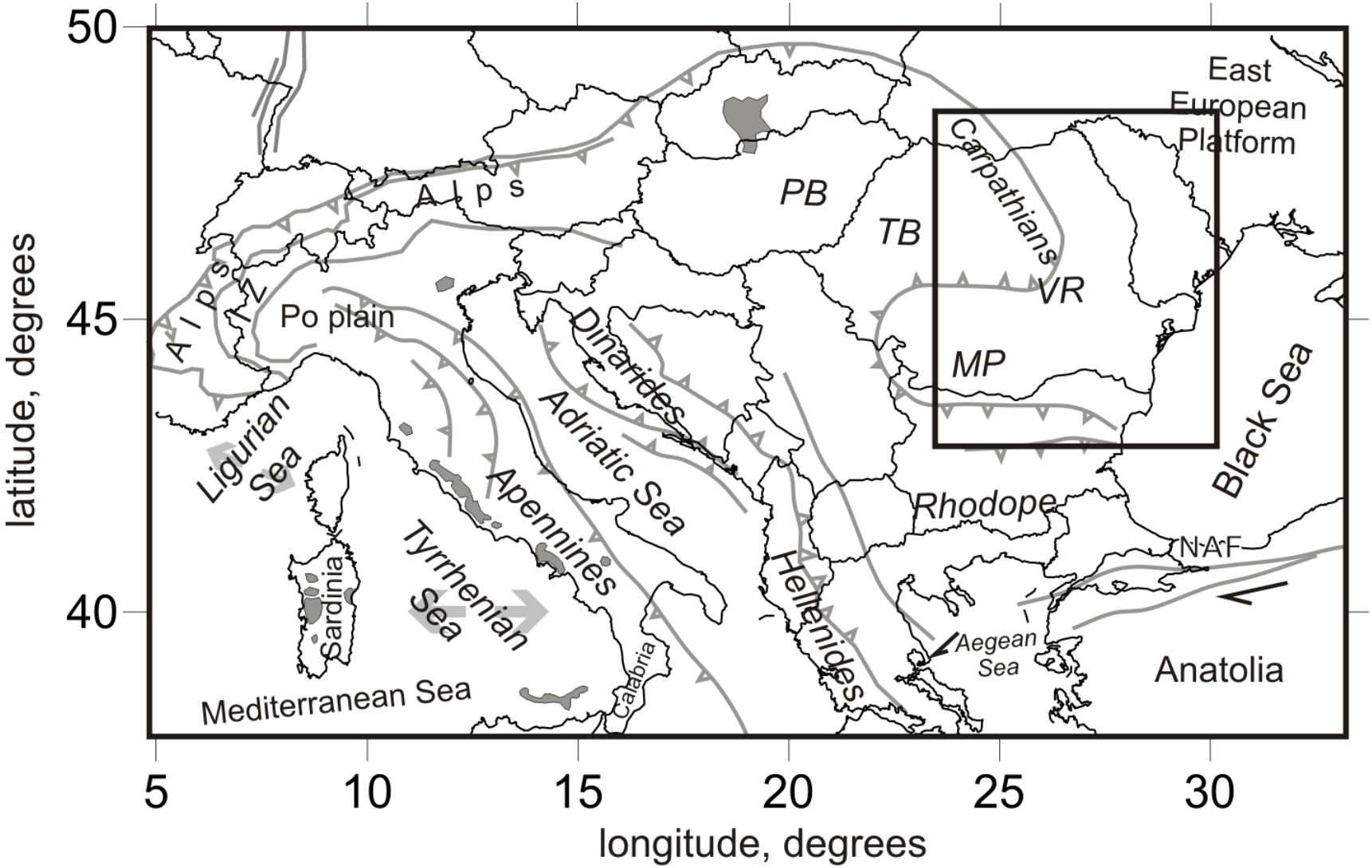

Figure 1. Main tectonic elements in Carpathian – Mediteranean region. The rectangle marks the area of interest for this study. Abbreviations: IZ – Ivrea Zone, MP – Moesian Platform, NAP – North Anatolian Fault, PB – Pannonian Basin, TB – Transylvania Basin, VR – Vrancea.

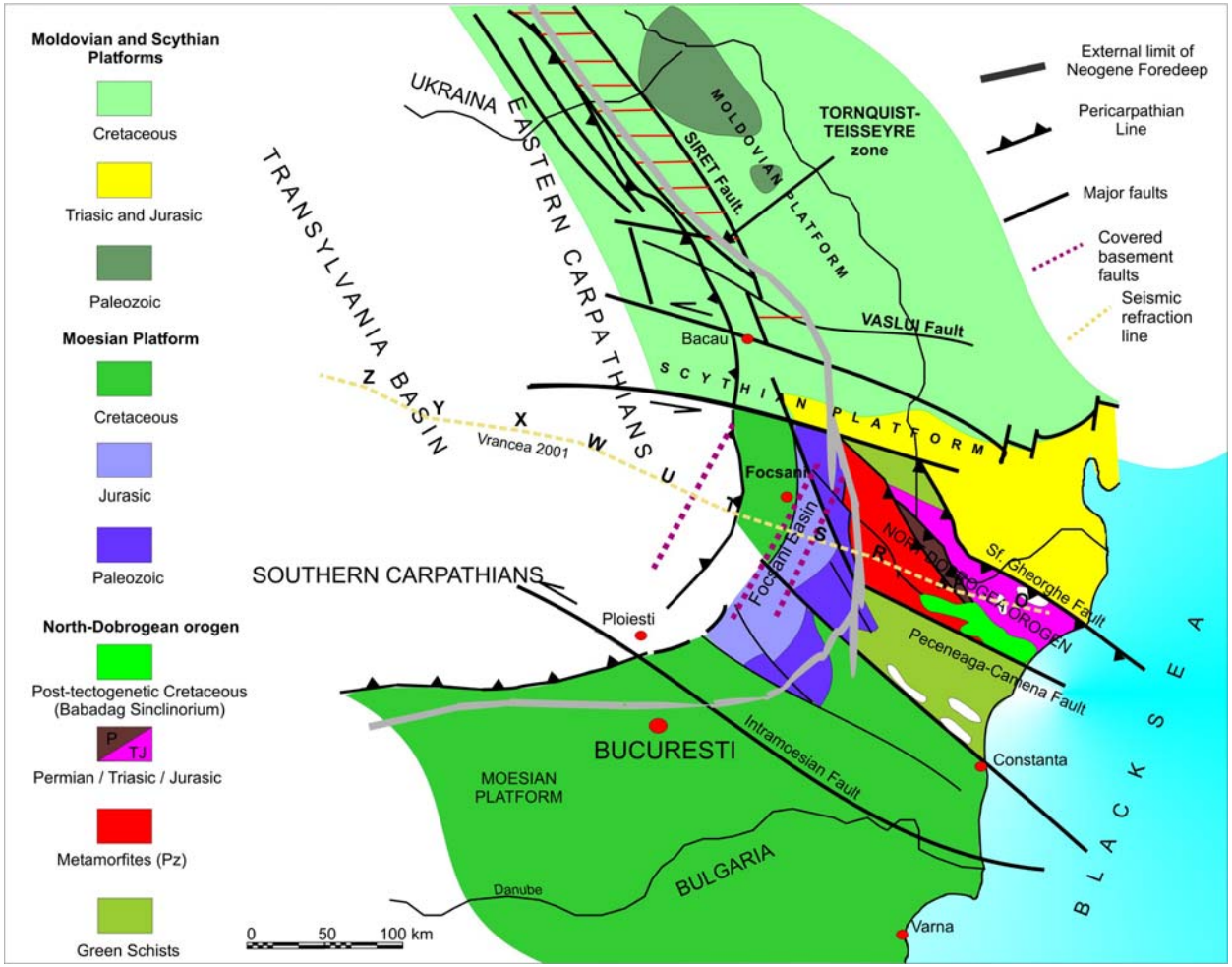

Figure2. Southeastern Carpathian arc bend tectonical map (modified after *Badescu*, 2005).

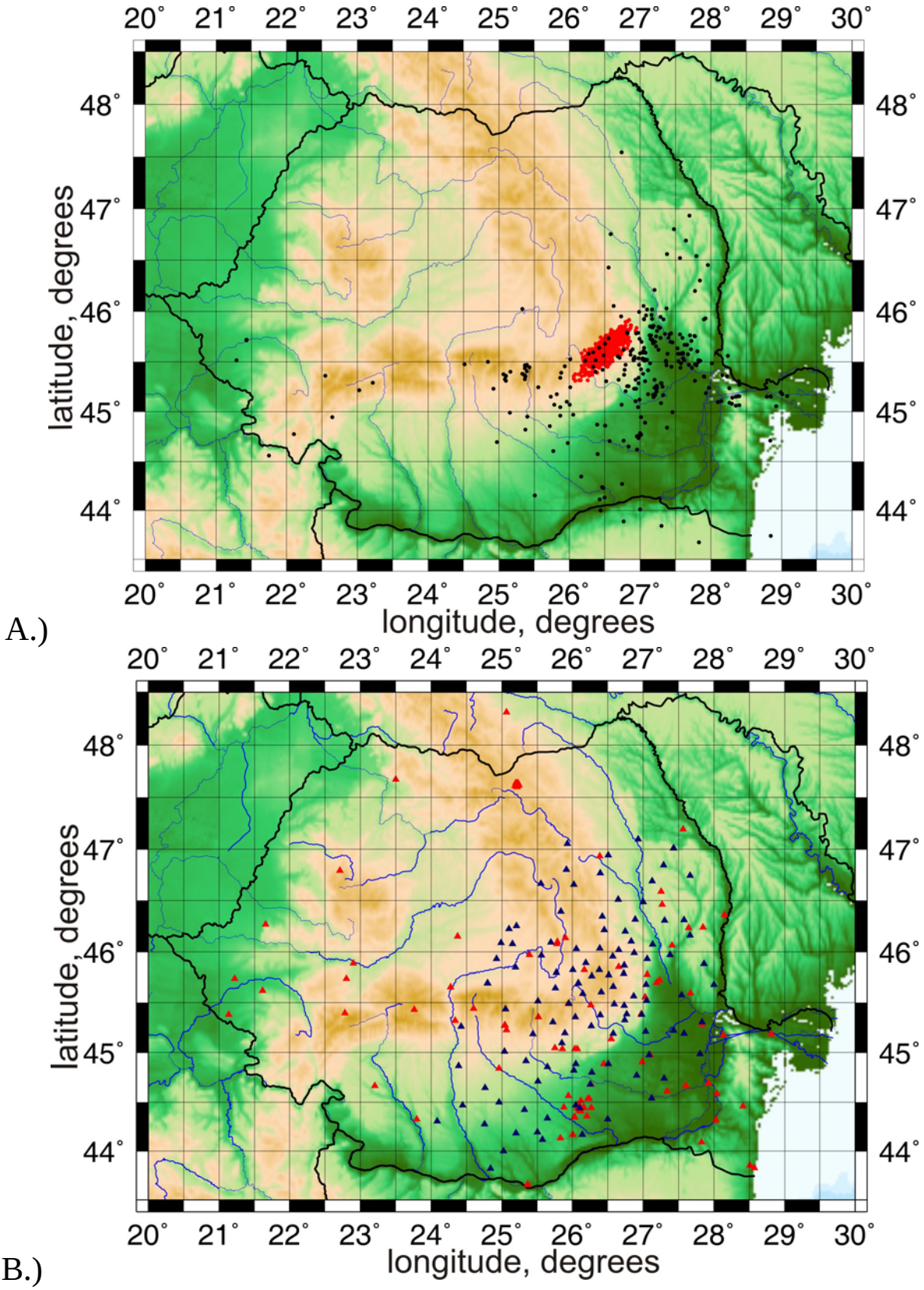

Figure 3. Data used in this study. A.) Earthquakes distribution. Red and black dots show intermediate-depth and crustal events, respectively. B.) Seismic stations: blue for temporary network from CALIXTO and red for stations which are sending data to RO-NDC.

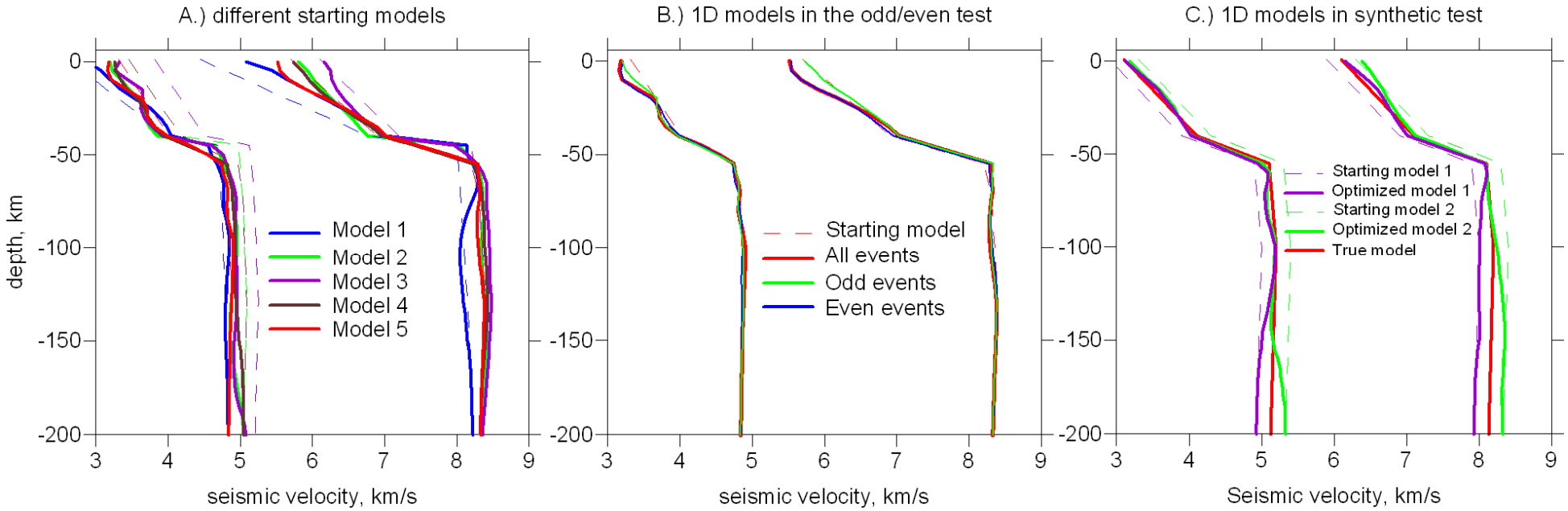

Figure 4. Optimization of the 1D model for observed and synthetic data. A.) Optimization results with observed data and different starting 1D models. Different colors indicate different models; dotted lines are the starting models; bold lines of corresponding colors are the optimization results. B.) optimization results for halved data subsets in the odd/even test. C.) Optimization results for synthetic data in the checkerboard test presented in Appendix 4.

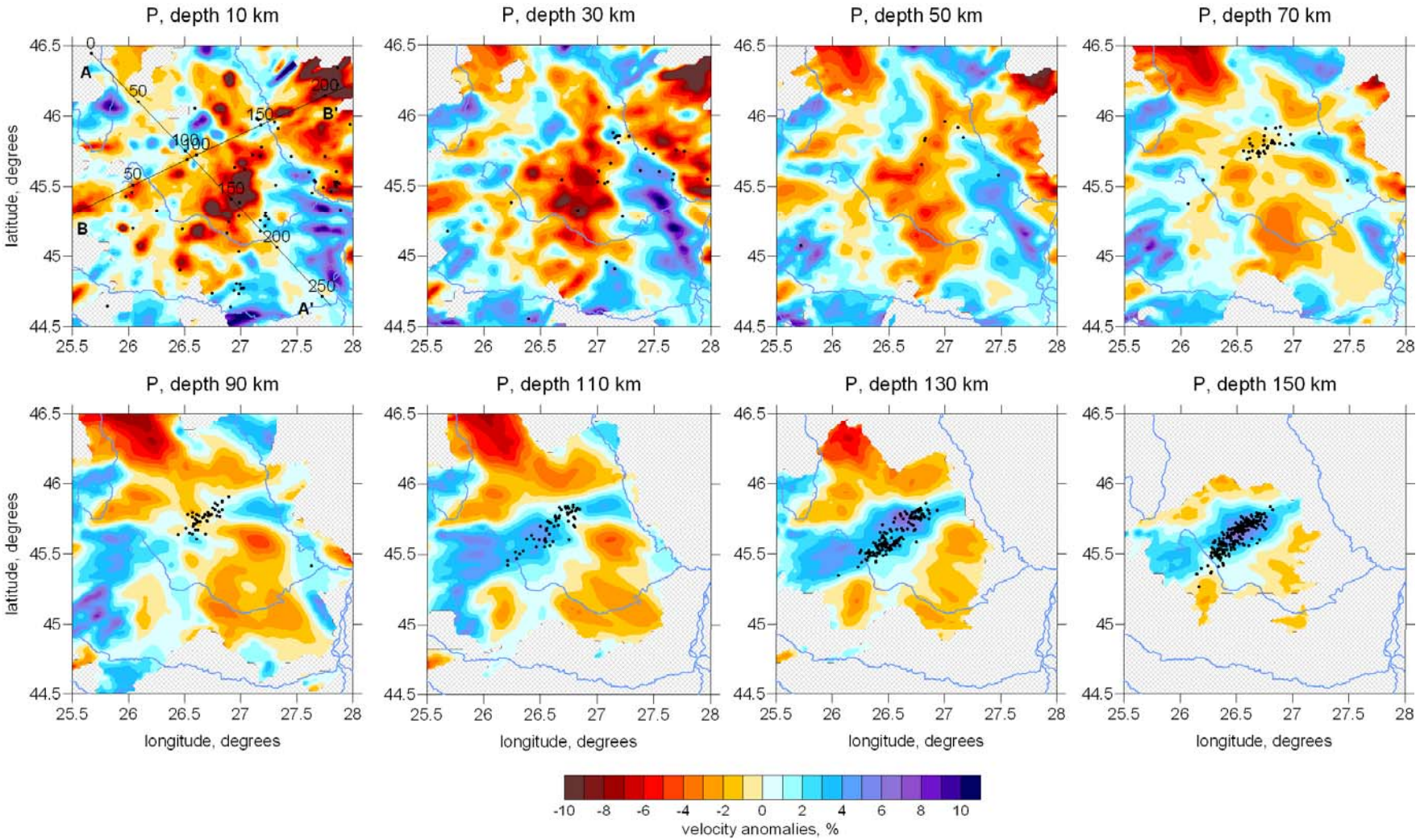

Figure 5. Horizontal sections of P velocity anomalies, in percent with respect to the optimized 1D velocity model, resulted from from the "Vp – Vs" inversion scheme. Dots depict the relocated sources around the corresponding depth levels. Locations of profile presented in Figure 7 are shown in section at 10 km depth.

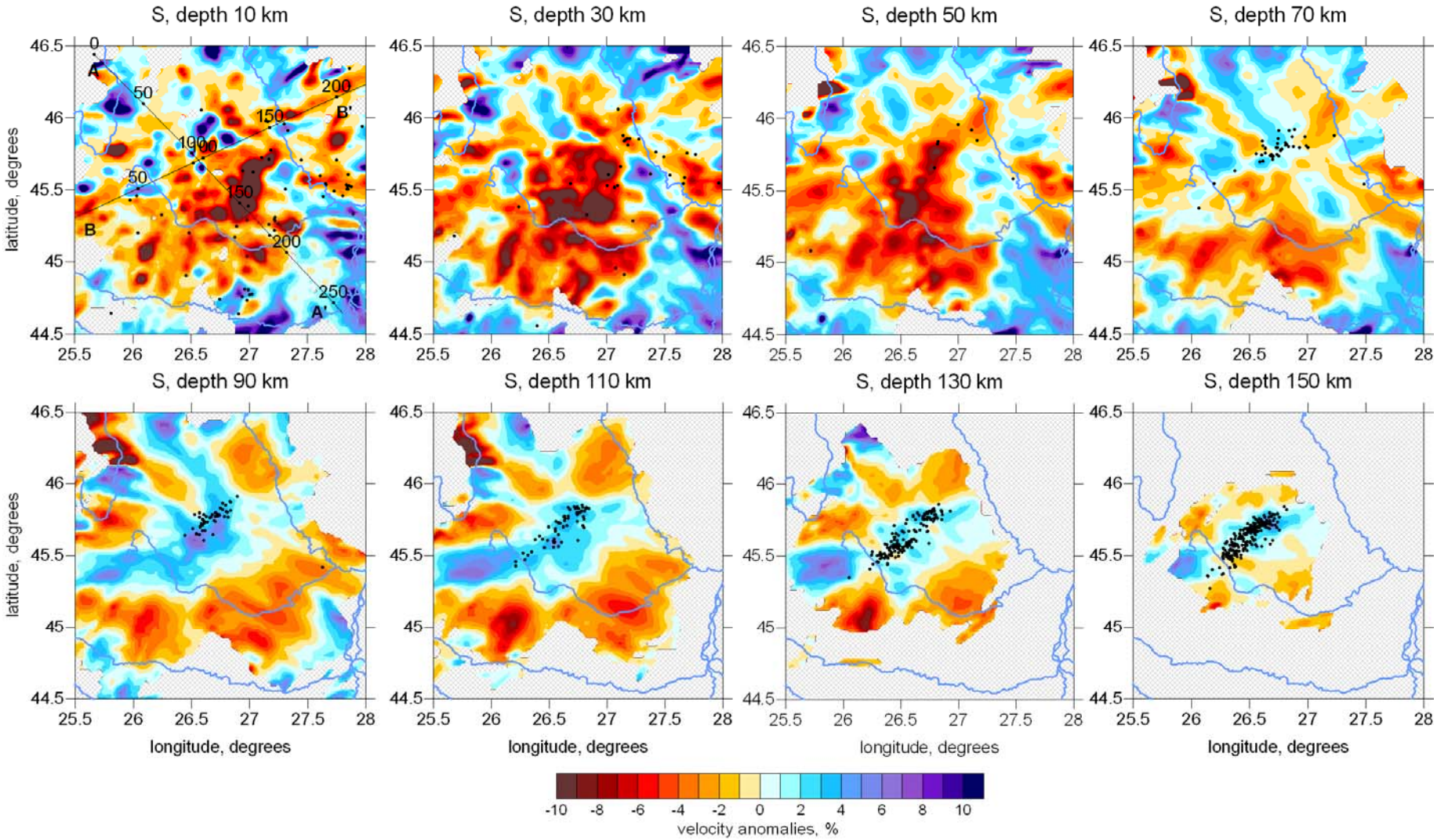

Figure 6. Same as Figure 5, but for the S velocity anomalies.

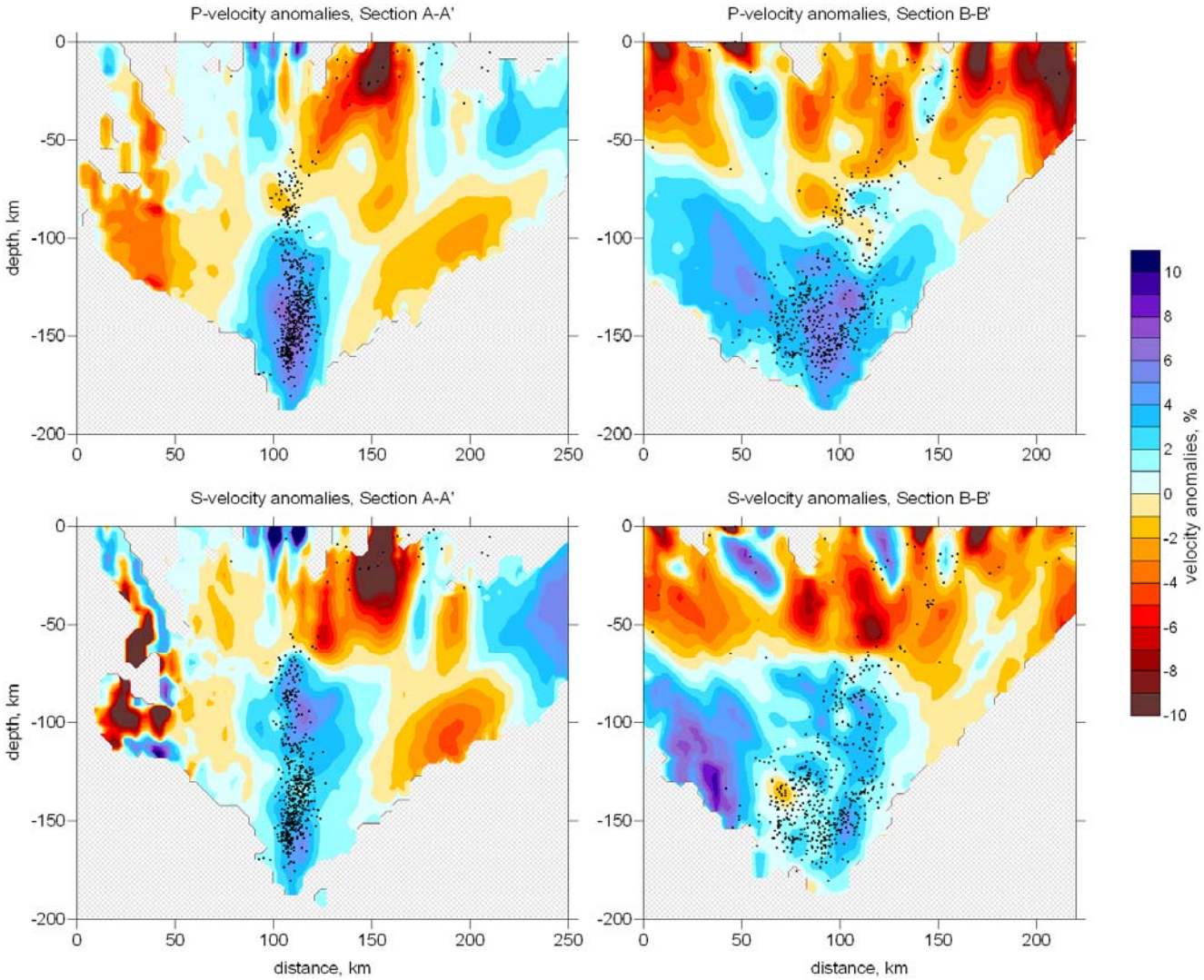

Figure 7. P and S velocity anomalies derived from the "Vp – Vs" inversion scheme in two vertical sections. Locations of the profiles are indicated in Figures 5 and 6. Dots depict the relocated sources at distances of less than 40 km from the profile.

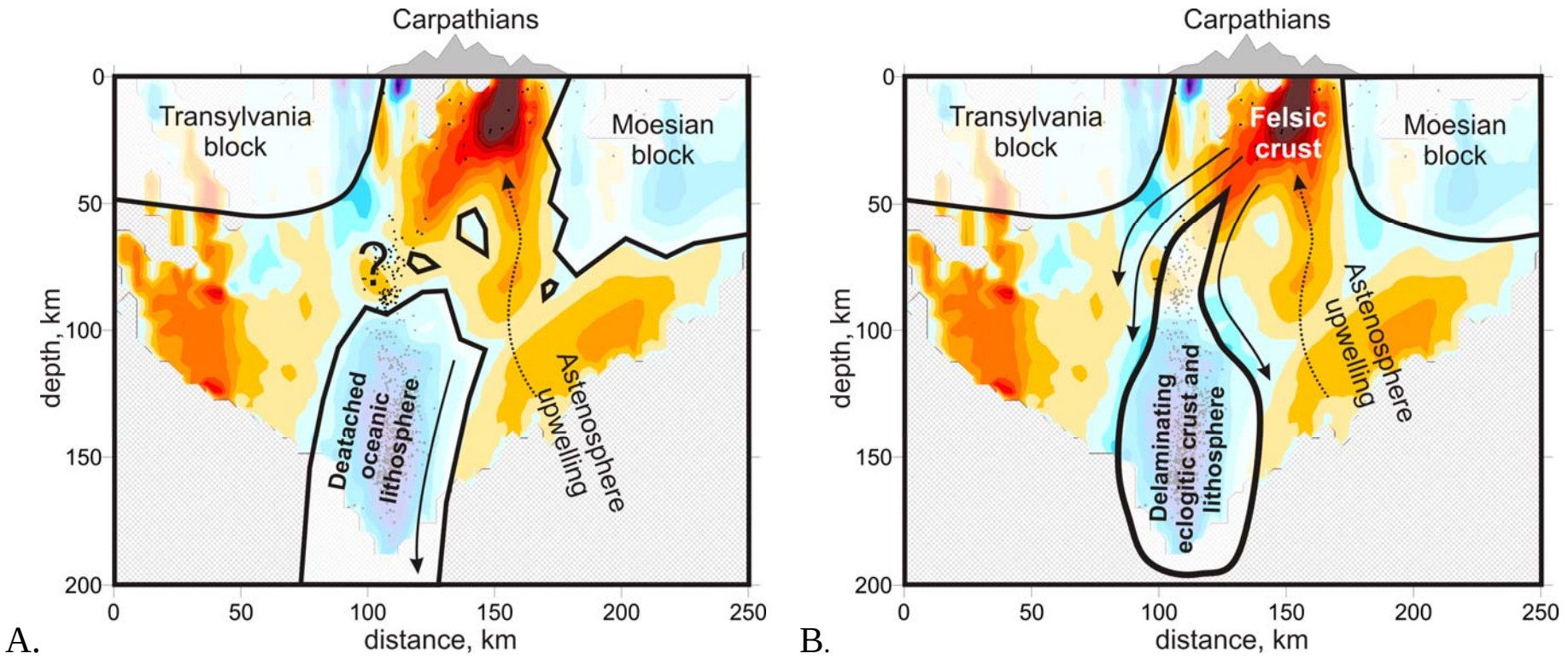

Figure 8. Interpretation cartoons based on the concept of subduction and slab detachment (Plot A), and delamination (Plot B). Background is the velocity distribution and events resulted from the tomographic inversion (P anomalies, Section A-A'), same as in Figure 7.

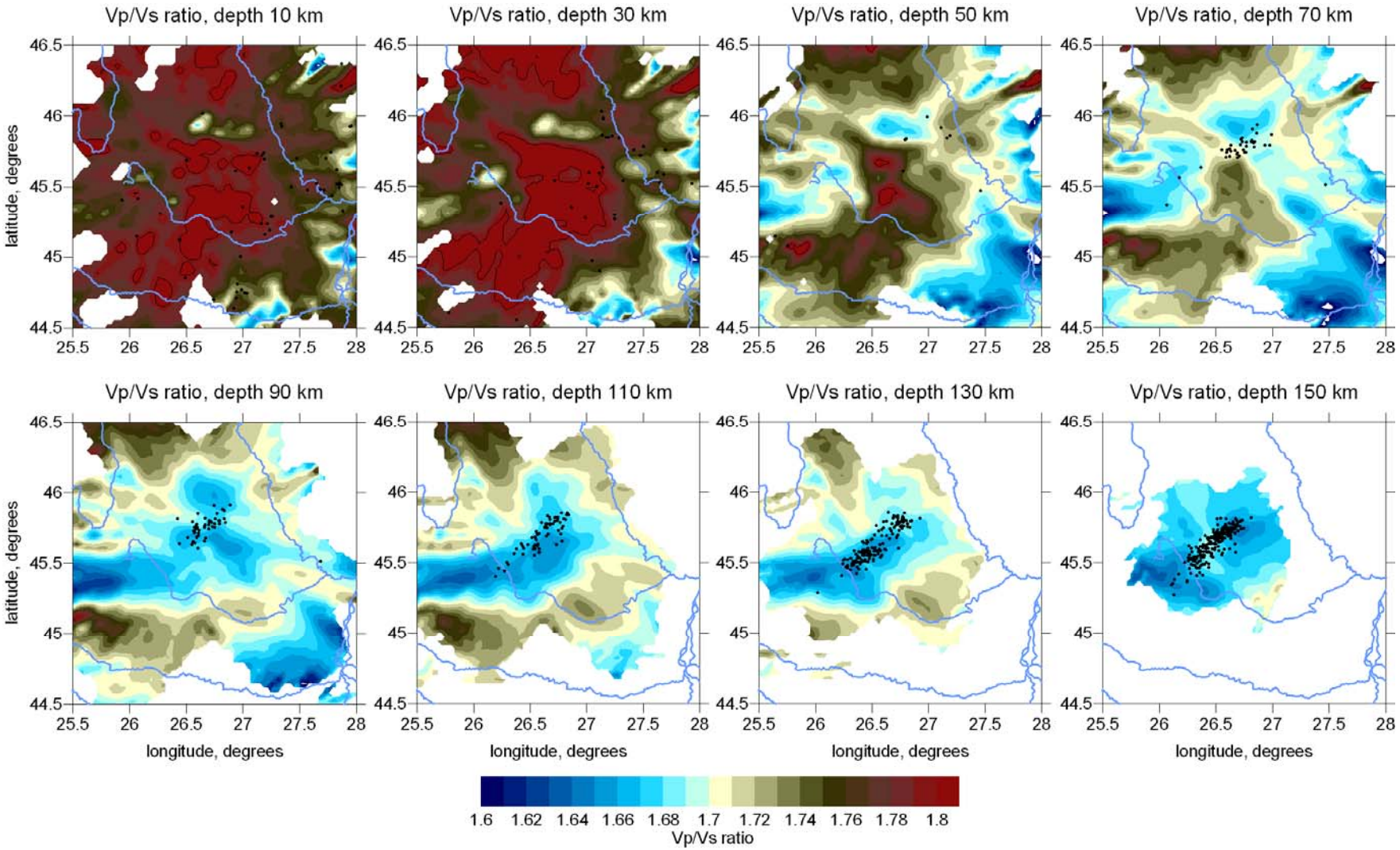

Figure A1. Vp/Vs ratio in horizontal sections derived from the “Vp - Vp/Vs” inversion scheme. Dots depict the relocated sources around the corresponding depth levels.

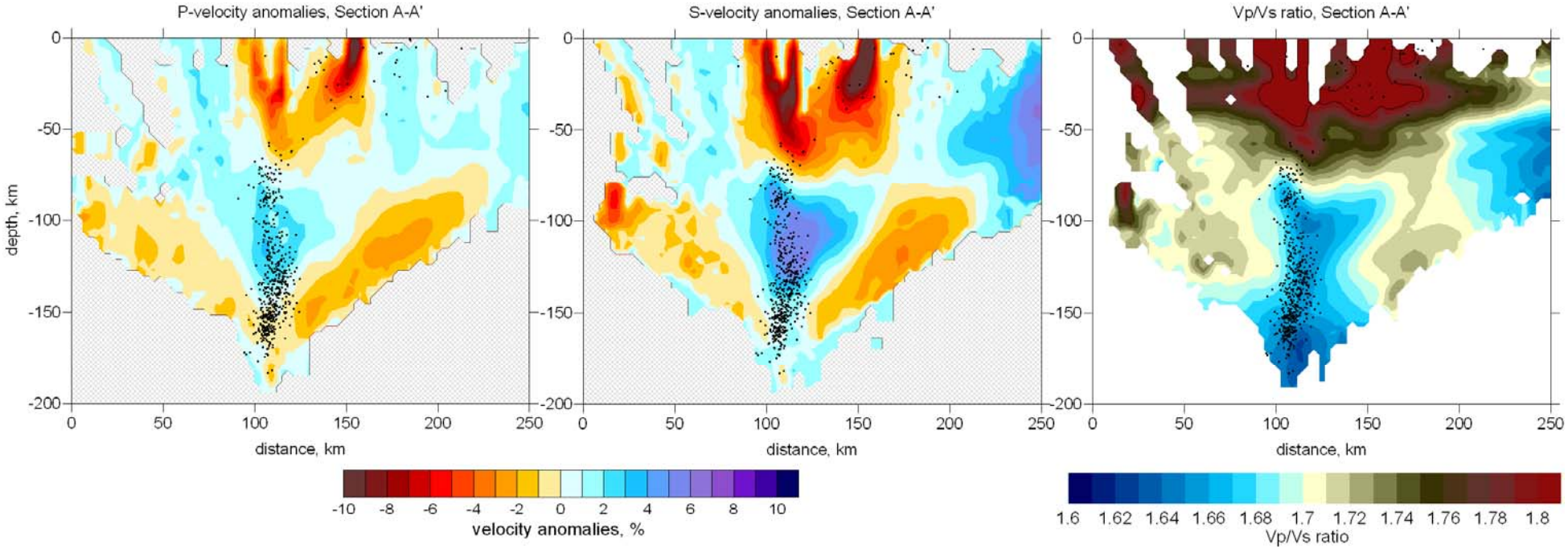

Figure A2. P and S velocity anomalies and Vp/Vs ratio derived from the "Vp - Vp/Vs" inversion scheme in the vertical section A-A' shown in Figure 5. Dots depict the relocated sources at distances of less than 40 km from the profile.

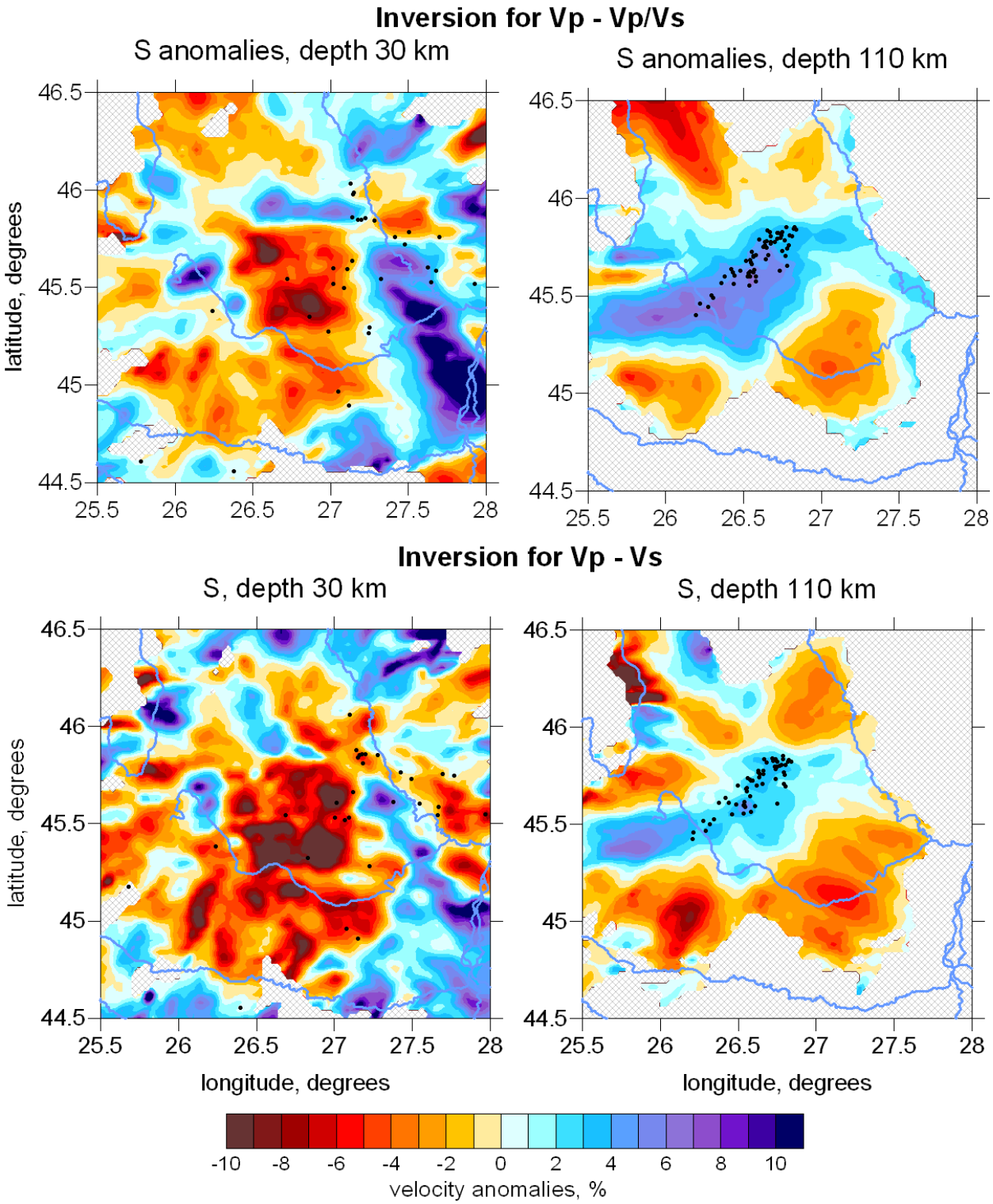

Figure A3. S velocity anomalies obtained using the inversion schemes for Vp - Vp/Vs (upper row) and for Vp-Vs (lower row) in two horizontal sections. Dots depict the relocated sources around the sections.

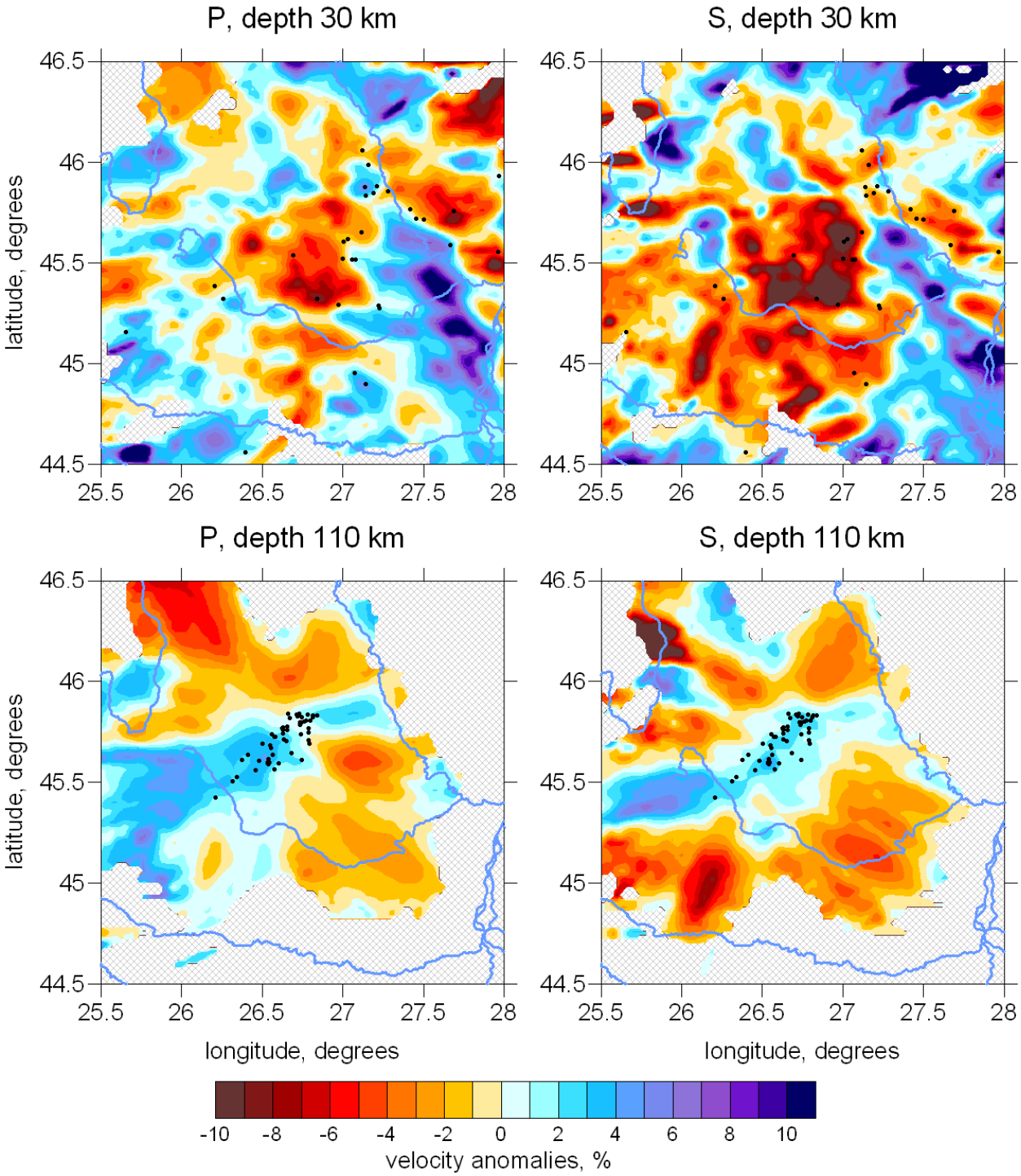

Figure A4. P and S velocity anomalies from Vp-Vs inversion based on another reference model. Dots depict the relocated sources around the sections.

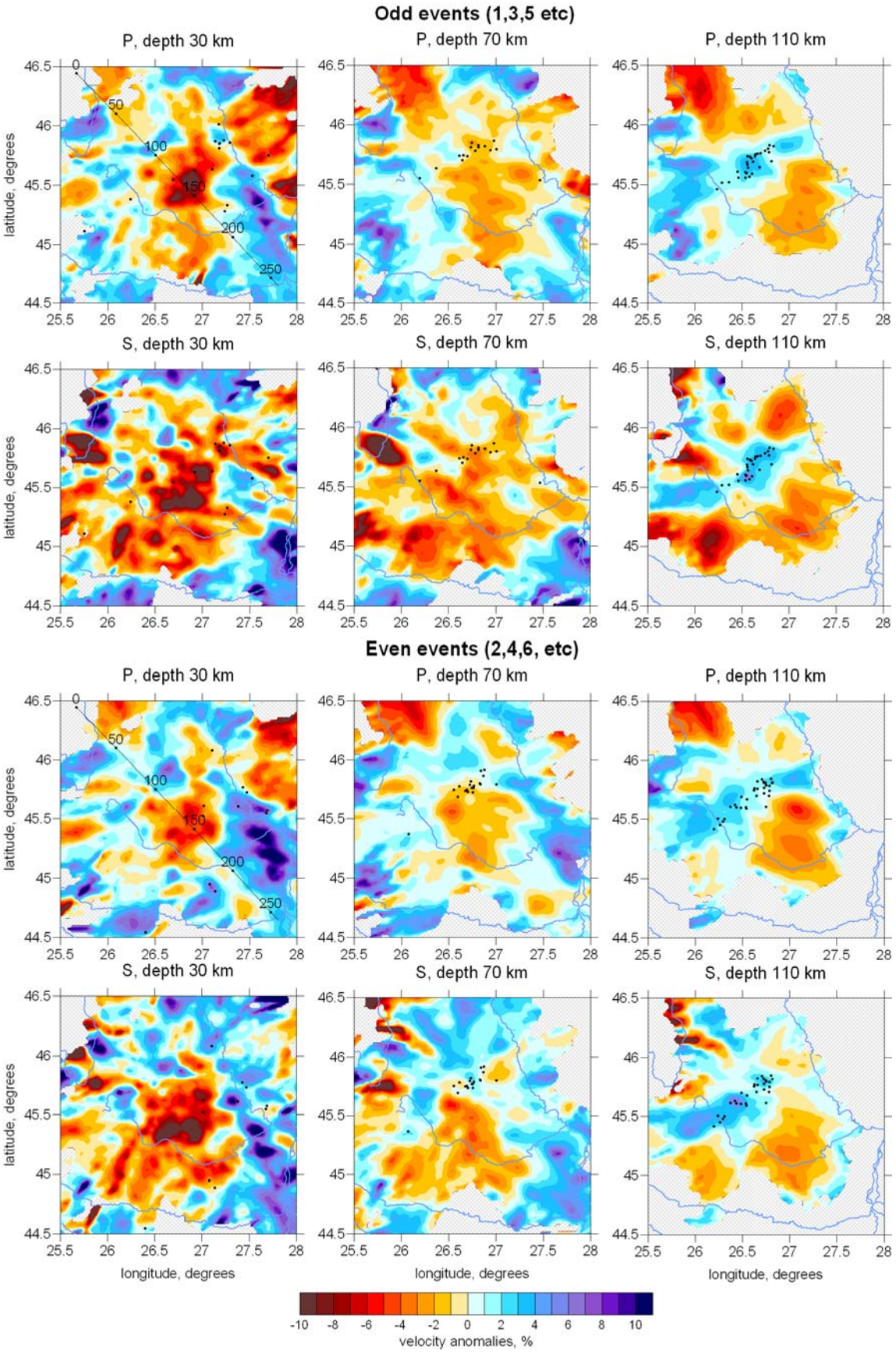

Figure A5. Odd-even test. Results for two halved subsets are presented for P and S anomalies in three horizontal sections. Dots depict the relocated sources around the sections.

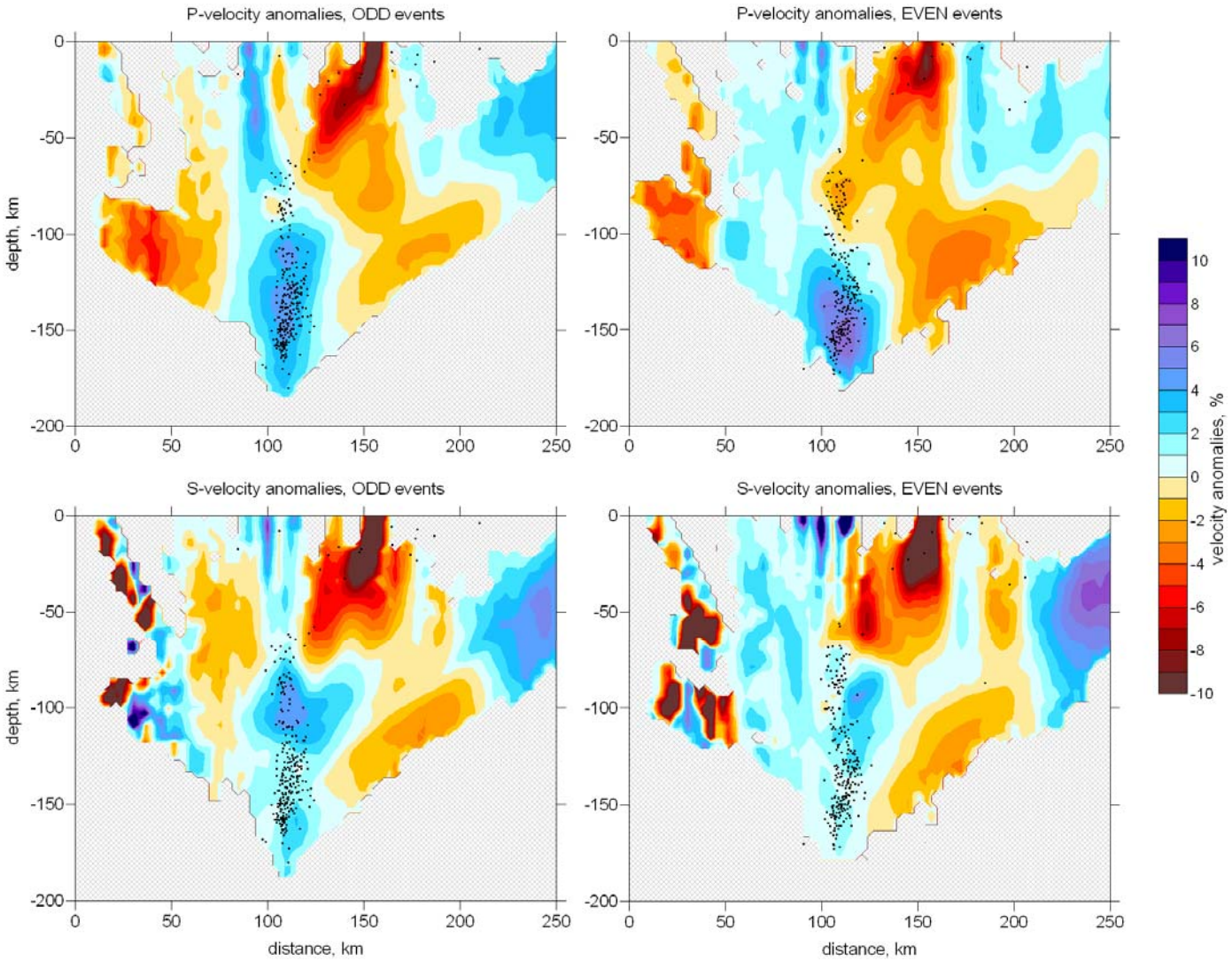

Figure A6. Same as Figure A5, but presented in a vertical section. Location of the section is indicated in Figure A5.

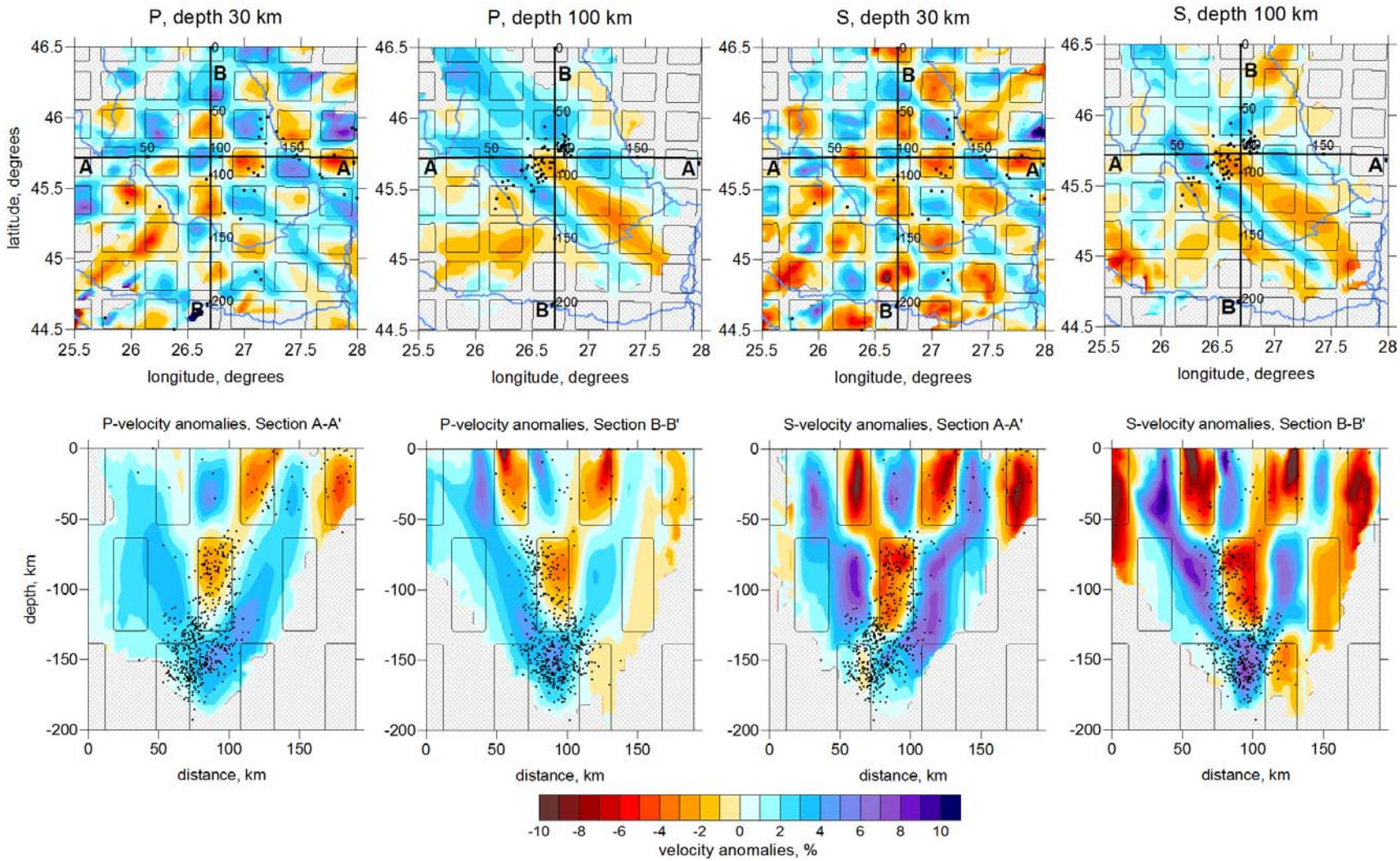

Figure A7. Checkerboard test performed according to Vp-Vs scheme in two horizontal sections (upper row) and two vertical sections (lower row). Initial synthetic patterns are highlighted with thin black lines. Locations of the profiles are indicated in all maps. Relocated sources are shown with black dots.

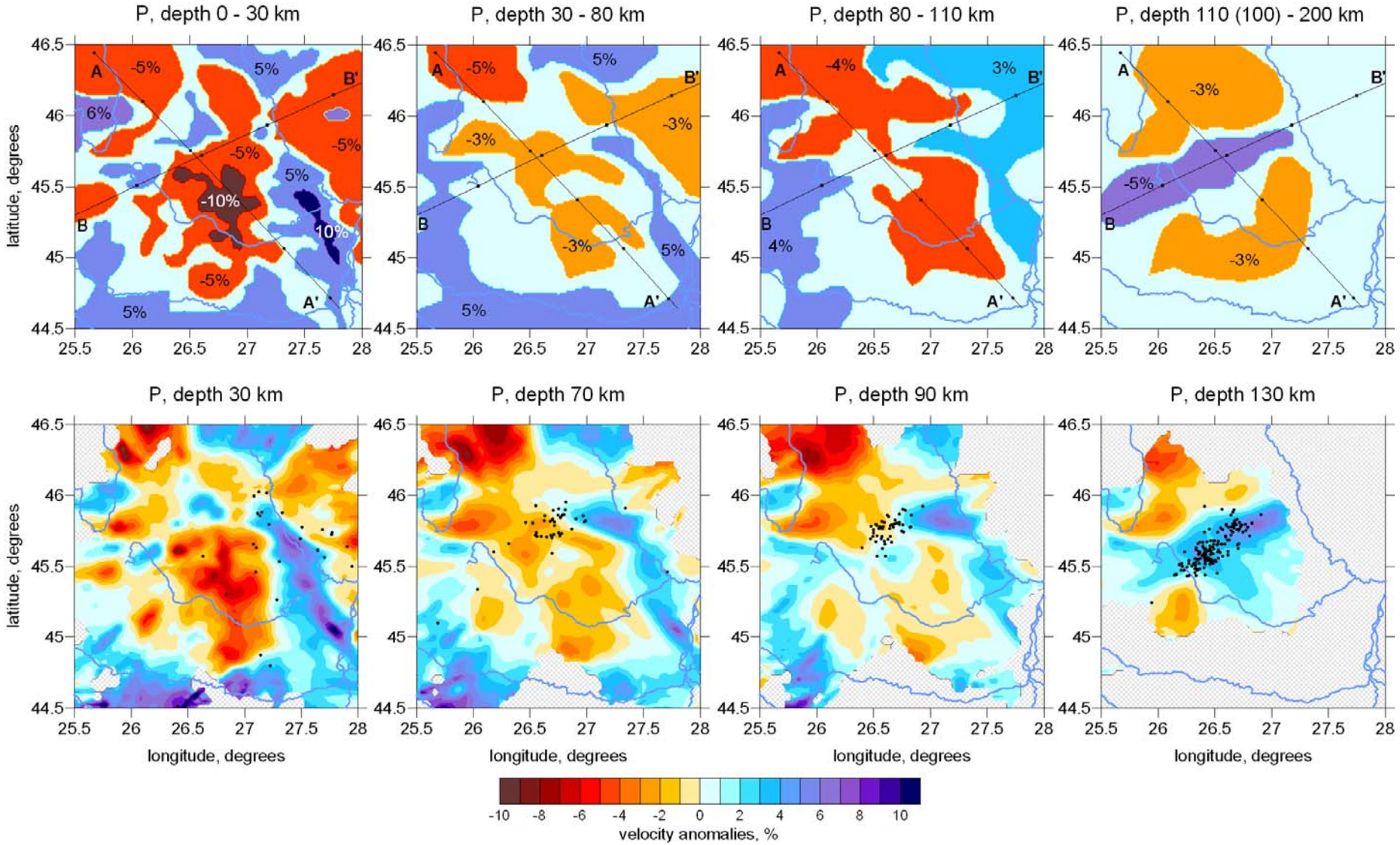

Figure A8. Synthetic test aimed at reproducing the results of the real experiment. Only results for P velocity modeling are shown in horizontal sections. Synthetic model defined in 3D prisms is shown in the upper row. Values of anomalies are indicated by nu anomalies; depth diapason of prism definition is given above each plot. Lower row shows reconstruction results for P velocity anomalies and source locations (black dots).

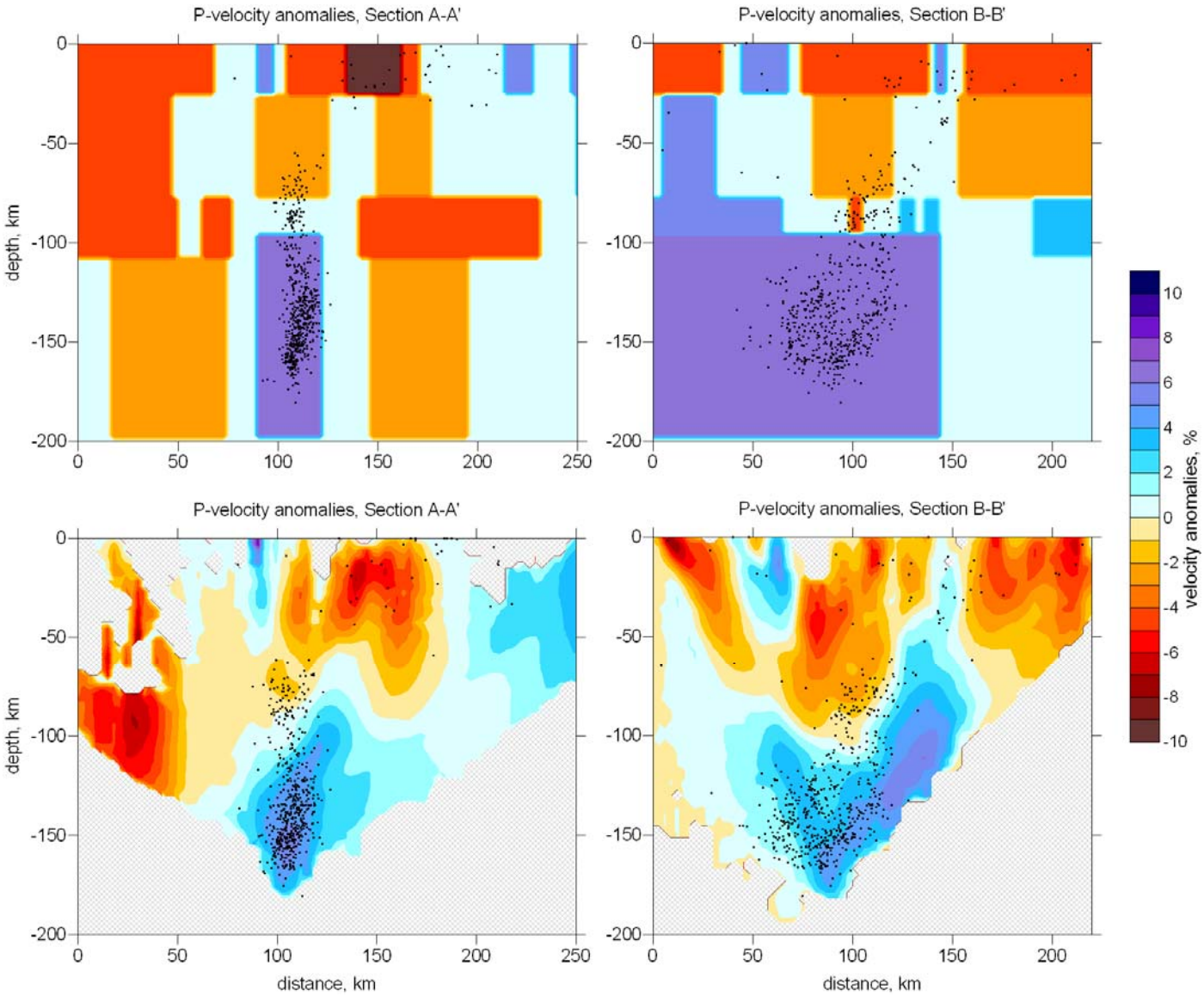

Figure A9. Same test as in Figure A8, but shown in two vertical sections A-A' and B-B' with locations indicated in the upper maps in Figure A8. Upper row represents P synthetic model; lower row is the reconstruction results for P velocity anomalies and source locations (black dots).